Enhanced Biogeochemical Cycling Along the U.S. West Coast Shelf

Pierre Damien, Daniele Bianchi, James Mcwilliams, Faycal Kessouri, Curtis Deutsch, Ru Chen, Lionel Renault

Global Biogeochemical Cycles

RESEARCH ARTICLE
10.1029/2022GB007572

Enhanced Biogeochemical Cycling Along the U.S. West Coast Shelf

Pierre Damien[1], Daniele Bianchi[1], James C. McWilliams[1], Faycal Kessouri[2], Curtis Deutsch[3], Ru Chen[4], and Lionel Renault[5]

[1]University of California, Los Angeles, Los Angeles, CA, USA, [2]Southern California Coastal Water Research Project, Costa Mesa, CA, USA, [3]University of Washington, Seattle, WA, USA, [4]Tianjin University, Tianjin, China, [5]Institut de Recherche pour le Developpement, Toulouse, France

Key Points:

- The biogeochemical balances along the U.S. West Coast shelf are characterized using a submesoscale-permitting oceanic biogeochemical model
- Alongshore wind stress, intensified curl, eddies, and boundary layer dynamics generate biogeochemical rates twice as large as offshore
- Intense mean and eddy cross-shore exchanges, mainly in the boundary layers, transport nutrients offshore, where they enhance productivity

Correspondence to:
P. Damien,
pdamien@ucla.edu

Citation:
Damien, P., Bianchi, D., McWilliams, J. C., Kessouri, F., Deutsch, C., Chen, R., & Renault, L. (2023). Enhanced biogeochemical cycling along the U.S. West Coast shelf. *Global Biogeochemical Cycles*, *37*, e2022GB007572. https://doi.org/10.1029/2022GB007572

Received 30 AUG 2022
Accepted 13 DEC 2022

Abstract Continental margins play an essential role in global ocean biogeochemistry and the carbon cycle; however, global assessments of this role remain highly uncertain. This uncertainty arises from the large variability over a broad range of temporal and spatial scales of the processes that characterize these environments. High-resolution simulations with ocean biogeochemical models have emerged as essential tools to advance biogeochemical assessments at regional scales. Here, we examine the processes and balances for carbon, oxygen, and nitrogen cycles along the U.S. West Coast in an 11-year hindcast simulation with a submesoscale-permitting oceanic circulation coupled to a biogeochemical model. We describe and quantify the biogeochemical cycles on the continental shelf, and their connection to the broader regional context encompassing the California Current System. On the shelf, coastal and wind stress curl upwelling drive a vigorous overturning circulation that supports biogeochemical rates and fluxes that are approximately twice as large as offshore. Exchanges with the proximate sediments, submesoscale shelf currents, bottom boundary layer transport, and intensified cross-shelf export of shelf-produced materials further impact coastal and open-ocean balances. While regional variability prevents extrapolation of our results to global margins, our approach provides a powerful tool to identify the dominant dynamics in different shelf setting and quantify their large-scale consequences.

1. Introduction

Oceanic margins—lying at the interface between the land, open ocean, atmosphere, and sediments—are emerging as central locations in Earth's Biogeochemical (BGC) transformations and exchanges, and an essential component of the land-to-ocean aquatic continuum (Regnier et al., 2022). Although this idea has a long history (Walsh, 1991), the most recent assessments exceed previous expectations, and reveal the critical role of margins in the global cycles of carbon (C), nutrients, and other elements (Cai et al., 2020; Fennel & Testa, 2019; Hofmann et al., 2011). Representing only about 7%–8% of the surface area of the oceans, shelf environments could support about 20% of total oceanic productivity, more than 40% of the carbon sequestration to the deep ocean, and at least 15% of the net uptake of atmospheric carbon dioxide (CO_2) by the global ocean (Cai, 2011; Dai et al., 2022; Laruelle et al., 2018; Muller-Karger et al., 2005). Because of the enhanced exchanges with land and atmosphere and large BGC rates, the effects of climate change are amplified along oceanic margins, adding to pressure from a growing human population along the coast (Breitburg et al., 2018; Cai et al., 2011; Doney et al., 2007; Lacroix, Ilyina, Mathis, et al., 2021; Regnier et al., 2013).

While there is a growing consensus on the importance of oceanic margins for global biogeochemistry (Fennel et al., 2008; Muller-Karger et al., 2005; Walsh, 1991), global assessments of this role remain uncertain (Hofmann et al., 2011), although observational and modeling advances have begun to close this gap (Fennel et al., 2019; Lacroix, Ilyina, Laruelle, & Regnier, 2021; Laruelle et al., 2014; Liu et al., 2021; Roobaert et al., 2019). The difficulty in quantifying ocean margin BGC cycles results from a combination of factors, including the small area of coastal regions, many of which remain undersampled compared to the open ocean; the variety of geographical conditions (e.g., Eastern vs. Western Boundary Currents, wide vs. narrow shelves, polar margins, etc.); the small spatial and temporal scales involved; and the presence of intense and often unique processes, including inputs from terrestrial and anthropogenic sources (Dai et al., 2022; Kessouri et al., 2021; Lacroix, Ilyina, Laruelle, & Regnier, 2021; Liu et al., 2021). Given these features, extrapolation from local to global scales is often fraught with uncertainties (Dai et al., 2022; Hofmann et al., 2011; Regnier et al., 2022). Progress toward

robust assessments of the role of continental margins at the global scale increasingly depends on improved estimates at regional and local scales (Bauer et al., 2013; Cai et al., 2020; Fennel et al., 2019; Najjar et al., 2018) and high-resolution modeling efforts (Dai et al., 2022; Liu et al., 2019; Regnier et al., 2022).

Among continental margins, the U.S. West Coast (USWC) comprises the California Current System (CCS), an ocean-dominated Eastern Boundary Upwelling that exhibits intense biological productivity and sustains high marine biodiversity and important fisheries (Chavez & Messié, 2009; McClatchie, 2014). In the CCS, the predominantly equatorward along-shore winds induce offshore surface Ekman transport balanced by upwelling of denser water at the coast, and shoreward flow at depth (Huyer, 1983; Marchesiello et al., 2003). Upwelled waters are rich in nutrients and dissolved inorganic carbon (DIC), and low in dissolved oxygen (O_2) and pH. Thus, while upwelling fuels high biological production, it also exposes shelf ecosystems to chemical conditions that are potentially harmful to a variety of organisms (Chan et al., 2008; Grantham et al., 2004; Gruber et al., 2012). Large biological DIC uptake in the CCS contributes to the global atmospheric CO_2 sink, while CO_2 outgassing in recently upwelled waters near the coast counteracts it in Central California (Feely et al., 2008; Fiechter et al., 2014; Landschützer et al., 2020; Laruelle et al., 2014).

Upwelling-driven surface density gradients and along-shore currents exhibit instability with highly energetic mesoscale and submesoscale eddy and frontal flows in the CCS (Capet et al., 2008; Marchesiello et al., 2003), which in turn affect BGC by transporting and subducting unutilized inorganic nutrients, detritus, and plankton offshore and downward along isopycnal surfaces (Chenillat et al., 2015; Deutsch et al., 2021; Nagai et al., 2015), in a process known as "eddy quenching" of productivity (Gruber et al., 2011; Lathuilière et al., 2010; Renault, Deutsch, et al., 2016). Submesoscale currents associated with strong surface density fronts, vigorous horizontal stirring, and intense vertical velocities in the upper layers (Capet et al., 2008; McWilliams, 2016; Thomas et al., 2008) further enhance BGC patchiness and modulate ecosystem responses (Kessouri, Bianchi, et al., 2020; Lévy et al., 2018).

Because of natural upwelling coupled to a slow decadal shoaling of the pycnocline (Deutsch et al., 2021), the CCS is expected to be at the forefront of emerging oceanic acidification and hypoxia driven by anthropogenic climate change (Chan et al., 2008; Feely et al., 2008; Gruber et al., 2012), resulting in a multitude of impacts on the coastal ecosystem (Doney et al., 2020; Marshall et al., 2017). A variety of studies, helped by long-running monitoring efforts (e.g., the CalCOFI program (McClatchie, 2014)), have begun showing evidence of these trends along the USWC (Bednaršek et al., 2014; Pespeni et al., 2013).

Although the CCS has been extensively studied, gaps remain in our understanding of BGC cycles in the region, especially on the shelf where acidification and hypoxia events are increasingly frequent (Chan et al., 2008; Feely et al., 2008; Fennel & Testa, 2019; Osborne et al., 2020). Despite knowledge that the bulk of upwelling occurs on the shelf, the patterns of shelf circulation, their contribution to BGC cycles, and their connection to the broad CCS remains poorly-quantified. Additionally, how sub-regional variability, submesoscale currents, and boundary-layer dynamics affect shelf circulation and BGC cycles coast-wide remain topics of active research (Fiechter et al., 2018; Kessouri, Bianchi, et al., 2020). These governing processes have often been studied separately, and how they balance each other in a consistent picture is still unclear. While model-based studies provide an ideal tool to study these questions (Dai et al., 2022; Frischknecht et al., 2018), shelf environments have often been poorly represented in models, because of the small scales and strong connections to the adjacent open ocean (Dai et al., 2022; Lacroix, Ilyina, Laruelle, & Regnier, 2021; Liu et al., 2019). Furthermore, cross-shelf exchange is often investigated too far offshore to realistically resolve the shelf-to-open ocean continuum (Lacroix, Ilyina, Laruelle, & Regnier, 2021; Liu et al., 2019; Regnier et al., 2022). This problem is particularly acute in the CCS, which is characterized by a narrow shelf with vigorous submesoscale activity (Dauhajre et al., 2017; Kessouri, Bianchi, et al., 2020; Kessouri et al., 2021).

Our goals with this study are two-fold: (a) elucidate how an intense, wind-driven overturning circulation enhances the cycles of carbon, nitrogen (N) and oxygen on the continental shelf of the USWC, and (b) elucidate the contribution of the continental shelf to the balances of these elements within the broader CCS, setting a standard for model-based assessments of BGC cycles along continental margins. Specifically, we aim to address the following questions: What physical and biogeochemical processes drive intense carbon, nutrient and oxygen cycles on the USWC shelf? What circulation patterns connect the shelf to the open ocean? And to what extent biogeochemical cycles on the shelf affect the adjacent open ocean? Answering these questions requires a faithful representation of the complex, fine-scale circulation and BGC of the region, and resolution of shelf processes and their

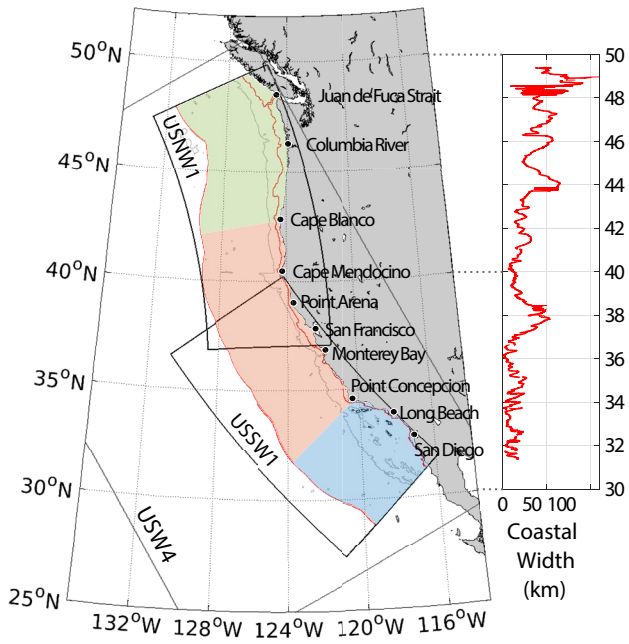

Figure 1. (a) Map of the USWC showing the 4 km resolution model domain (USW4, gray box) and the twin 1 km resolution northern (USNW1) and southern (USSW1) domains (black boxes). The 200 m isobath (inner red line) divides the oceanic margin from the offshore CCS extending approximately 400 km away from the coast (outer red line). The 2,000 m isobath (light gray line) illustrates the steepness of the continental slope. The CCS is separated into three regions: the Southern Region south of Point Conception (blue shading); the Central Region between Point Conception and Cape Blanco (red shading); and the Northern Region north of Cape Blanco (green shading). (b) Width of the continental shelf (km) between 0 and 200 m depth, as a function of latitude (red line).

connection to the open ocean. These elements are also needed to improve predictions of BGC and ecosystem change in the CCS (Brady et al., 2020; Jacox et al., 2014), and to expand our understanding of the role of continental margins in the global BGC cycles and changes now underway (Doney, 2010; Regnier et al., 2022; Stock et al., 2020). Ultimately, the purpose of this paper is to provide a revised picture of BGC cycles along the USWC, and set a new standard for studies of climate change and anthropogenic impact on continental margin systems.

To this end, we present results from a twin set of high-resolution (i.e., submesoscale-permitting) numerical simulations, composed of a Southern and a Northern configuration that span the USWC (Figure 1). The simulations are integrated over a 11-year period, forced by realistic winds that include the orographic shaping of the atmospheric boundary layer (Fiechter et al., 2018; Renault, Hall, & McWilliams, 2016) and current feedback to the wind stress (Renault, Molemaker, et al., 2016; Renault et al., 2020), both major physical drivers along the USWC. They are nested in a mesoscale-resolving parent simulation at coarser resolution (Deutsch et al., 2021; Renault et al., 2021) that conveys the external influences of the wind-driven gyres and broader CCS into the fine-scale processes along the coast. The simulations fully resolve the mesoscale circulation and provide a partial representation of submesoscale currents along a narrow shelf over an unprecedented time period and spatial extent (Kessouri, Bianchi, et al., 2020). This expensive numerical approach is expected to advance coastal modeling toward improved realism, and to provide time series long enough for statistically robust analyses of local scale variability.

The rest of the paper is organized as follows. Section 2 describes the methods, including model setup and analysis approach. Section 3 provides an overview of the physical circulation, BGC distributions and cycling rates along the USWC, focusing on the balances of carbon, nitrogen and oxygen, with emphasis on the cross-shelf overturning and shelf-to-offshore connectivity. Section 4 provides a detailed analysis of the cycles of these elements on the shelf, and their offshore transports. Section 5 discusses the main findings of the study and their relevance to the broader topic of continental margin biogeochemistry. Various appendices provide additional information to support our results.

2. Methods

2.1. The Coupled Circulation—Biogeochemical Model

Our approach is based on the online coupling between the Regional Ocean Modeling System (ROMS, Shchepetkin & McWilliams, 2005) and the Biogeochemical Elemental Cycling model (BEC, Deutsch et al., 2021; Moore et al., 2004). The model solutions analyzed here are run on two Arakawa C grids that cover the whole USWC, from Baja California to Vancouver Island, with a horizontal resolution of about 1 km, that is, submesoscale-permitting (Capet et al., 2008; Kessouri, Bianchi, et al., 2020), and with 60 topography-following vertical levels irregularly stretched for better surface and bottom resolution. The stretching parameters are h_{cline} = 250 m, θ_b = 3.0, and θ_s = 6.0 (Shchepetkin & McWilliams, 2009). The southern configuration (USSW1) extends from 130.7°W to 115.9°W and from 24.4°N to 40.2°N (from Tijuana to Cape Mendocino, Figure 1). The northern configuration (USNW1) extends from 133.0°W to 121.5°W and from 36.8°N to 49.9°N (from Monterey Bay to Vancouver Island, Figure 1).

Initial and boundary conditions for both simulations are provided by downscaling an existing hindcast simulation for the whole USWC run at 4 km (USW4) with the same model configuration (Deutsch et al., 2021; Renault et al., 2021). The physical surface forcings are identical to the "parent" 4 km simulation and consist of radiative, momentum, heat, and freshwater fluxes at the air-sea interface computed from hourly output from a 6 km

resolution atmospheric simulation with the Weather Research and Forecast model (Skamarock et al., 2008) using bulk formulas (Large, 2006). The topography is retrieved from Becker et al. (2009) at 30 arc s, and smoothed to limit horizontal pressure gradient errors. Further details on the 4 km configuration setup, initialization, and boundary forcings can be found in Deutsch et al. (2021) and Renault et al. (2021), along with an extensive validation of the large-scale circulation and BGC solutions. We also refer the reader to Kessouri, Bianchi, et al. (2020) for a discussion of the emergence of submesoscale physics and its BGC effects in the USSW1 simulation.

The two configurations are run over an 11-year period, starting in October 1996 and ending in December 2007. Physical and BGC state variables are saved as daily averages; physical fluxes and BGC rates as monthly averages. To provide a robust picture of the typical state of the CCS, model output is analyzed over a 8-year period (1999–2007) that excludes year 1998, known for its particularly intense El Niño (Friederich et al., 2002). To a remarkable degree, there is good continuity for the statistical properties of the solutions in the overlap region for USSW1 and USNW1 (Figure 1).

2.2. BGC Material Balance Equations

We compute the balances of organic carbon (OC, consisting of living, dissolved, and detrital components), DIC, inorganic nitrogen (IN, the sum of nitrate NO_3^-, nitrite NO_2^-, and ammonium NH_4^+), and O_2 along the USWC, based on monthly climatologies. The balance equations for these tracers can be summarized as follows:

$$\frac{\partial OC}{\partial t} = Adv_{OC} + Mix_{OC} + PP_C - Remin_C - Pexp_{OC} \quad (1)$$

$$\frac{\partial DIC}{\partial t} = Adv_{DIC} + Mix_{DIC} - PP_C + Remin_C + Sed_C + AIF_{CO2} \quad (2)$$

$$\frac{\partial IN}{\partial t} = Adv_{IN} + Mix_{IN} - PP_N + Remin_N + Sed_N \quad (3)$$

$$\frac{\partial O_2}{\partial t} = Adv_{O_2} + Mix_{O_2} + PP_{O_2} - Resp - Sed_{O_2} + AIF_{O_2} \quad (4)$$

In these equations, PP_x and $Remin_x$ represents respectively the effects of primary production and remineralization of the element x, linked together by a fixed stoichiometry ($C : N : O_2 = 117{:}16{:}{-}150$). $Resp$ represents oxygen consumption by respiration and nitrification, Sed_x is the flux from sediment, $Pexp_{OC}$ is the organic carbon export by settling particles (which in the model are instantaneously redistributed to the remineralization term), and AIF_x is the air-sea flux of CO_2 and O_2. Adv_x and Mix_x represent physical transports by advection and parameterized vertical diffusion respectively. Adv_x is computed using the third-order upwind scheme described in Marchesiello et al. (2009) and Lemarié et al. (2012), and Mix_x is specified by the K-profile Parameterization (KPP) boundary-layer scheme (Large et al., 1994). By averaging these balance term equations over 8 years, the temporal derivatives nearly vanish, allowing analysis of the BGC seasonal steady-state dynamics of the CCS. Seasonal variability is then quantified by constructing monthly climatological averages of each term in the balance equations.

For a complete description of BEC model's equations and parameters, we refer the reader to Deutsch et al. (2021), in particular the Appendix. Unless differently stated, we restrict the BGC balance analysis to the upper 0–50 m layer, which corresponds to the approximate range of the euphotic zone and encompasses the maximum mixed layer depth in the CCS.

2.3. Eddy Decomposition of Biogeochemical Transport

To highlight the importance of eddies on the transport of biogeochemical material, we separate the advective terms of Equations 1–4 into mean and eddy components, following a classical Reynolds decomposition:

$$\overline{uA} = \overline{u}\,\overline{A} + \overline{u'A'}, \quad (5)$$

where u is the cross-shore velocity, and A the concentration of a particular biogeochemical tracer. The overbar represents a monthly mean operator and ' the deviation from this mean. Practically, $\overline{uA}$, $\overline{u}$, and $\overline{A}$ are computed

online, and the eddy term is retrieved by difference. This decomposition has been used in previous studies (Capet et al., 2008; Gruber et al., 2011; Kessouri, Bianchi, et al., 2020; Nagai et al., 2015) to investigate eddy-induced transport. Here, we use it to quantify the eddy contribution to shelf overturning and shelf-to-offshore exchanges. The resultant eddy components include transport on time scales faster than a month, that is, mesoscale and submesoscale fluctuations. Critically, the importance of eddy transport on shelf BGC balances remains largely unresolved in current models targeting continental margins (Dai et al., 2022; Lacroix, Ilyina, Laruelle, & Regnier, 2021; Liu et al., 2019), although it is likely to play a primary role.

2.4. Along-Isobath Coordinate Transformation

For convenience, we define the continental shelf as the region with a topographic depth shallower than 200 m (Laruelle et al., 2013). Along the USWC, the width of the continental shelf, estimated from the smoothed topography, varies considerably with latitude around a mean value of 25 km, but it rarely exceeds 50 km (Figure 1). The USWC continental margin is particularly narrow south of Monterey Bay (∼10 km on average), where a horizontal resolution of 1 km or less is required to resolve shelf physical processes.

To highlight the vigorous cross-shelf overturning circulation and the resulting BGC intensification, and to facilitate visualization and analysis of model output, we remap model variables on a curvilinear, along-isobath coordinate system adapted to the USWC. This coordinate system is based on 3-dimensional (excluding time) locally orthogonal planes, with the $\vec{y}$ axis aligned with the 200 m isobath and pointing poleward, and the $\vec{x}$ axis pointing shoreward, representing the primary direction of the bathymetric gradient. Further offshore, that is, for depths greater than 200 m, we transition to a more typical curvilinear coordinate system, with the same $\vec{y}$ axis, but using distance from the 200 m isobath as the $\vec{x}$ axis. The latter extends 400 km offshore and embraces the entirety of the California Current and its meanders. In a region dominated by coastal upwelling and anisotropic circulation, this is a convenient coordinate system that naturally highlights gradients in the cross-shore and along-shore directions, and allows a clear characterization of coastal processes on the narrow shelf.

3. BGC Cycles Along the USWC

3.1. Mean Shelf Circulation and Overturning

The CCS is typically described as a wide Eastern Boundary Current, which comprises an offshore equatorward flow at the surface, nearshore summer-intensified wind-driven upwelling, a vigorous cross-shore overturning circulation, and the subsurface poleward California undercurrent hugging the continental slope around the 200 m isobath (Checkley & Barth, 2009; Hickey, 1979; Huyer, 1983; Marchesiello et al., 2003; Molemaker et al., 2015). In summertime, a coastal equatorward current forms on the shelf to geostrophically balance the cross-shore density gradient produced by upwelling. These circulation patterns are well captured by our solutions (Figure 2).

To highlight regional variations, we separate the CCS into Southern, Central, and Northern Regions, each characterized by coherent and distinct features (Figure 1; see also Appendix A for further details), consistent with previous work (Fiechter et al., 2018; Hales et al., 2012; Renault, Hall, & McWilliams, 2016; Turi et al., 2014). The Southern Region, south of Point Concepcion, comprises the complex bathymetry, islands, and channels of the Southern California Bight, and is characterized by cyclonic recirculation and weaker upwelling. The Central Region, spanning Central and Northern California, is more directly exposed to the offshore oceanic circulation and intense summer upwelling. Finally, the Northern region comprises the Oregon and Washington coasts, and is separated from the Central Region at Cape Blanco, north of which the prevailing winds drive downwelling in winter and upwelling in summer (Figures A1c).

Figure 2 shows that across the USWC, the wind stress curl is enhanced on the shelf, with a peak in the very nearshore region (shallower than 100 m depth), and it quickly vanishes further offshore. In this simulation, cross-shore gradients in winds are resolved by using forcings from an atmospheric model simulation run at 6 km resolution (Renault et al., 2021). The so-called wind drop-off zone (Fiechter et al., 2018; Renault, Hall, & McWilliams, 2016) drives a surface Ekman transport divergence, which is balanced by a cross-shelf flow at depth that feeds into the upwelling/downwelling on the shelf.

Because of the steep decline of the wind stress curl offshore, the wind-forced (Figure A1c) vertical circulation occurs mostly on the shelf, turning the whole continental margin into the "engine" of wind-driven upwelling.

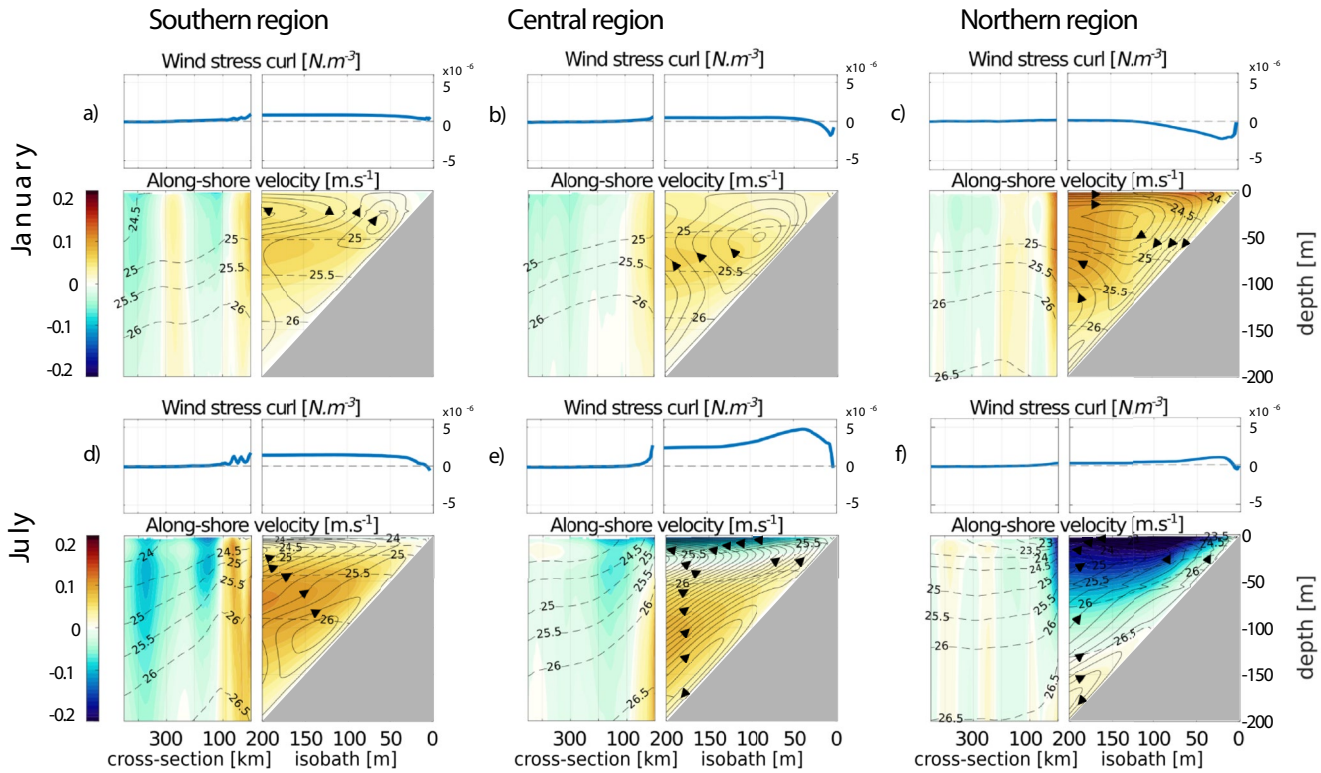

Figure 2. Along-shore (color shading) currents in the U.S. West Coast, averaged in time for the months of January (a, b, c) and July (d, e, f), and in space along a direction parallel to the coast, for the Southern (a, d), Central (b, e), and Northern (c, f) Regions. By convention, northward along-shore currents are shown by positive velocities (orange colors), and southward by negative velocities (blue colors). As described in Section 2.4, the left side of the *x*-axis in each panel indicates isobaths in meters, while the right side shows the distance form the shelf in kilometers. On the shelf, black solid streamlines show a "pseudo" stream function ($\Psi_{\beta z}$) computed in the isobath-depth coordinate system as $\partial\Psi/\partial x = w$, with w the along-shore averaged vertical velocity set to 0 on the shelf bottom, used to diagnose the cross-shelf overturning circulation. Dashed black contours show isopycnal surfaces with labeled potential density anomalies. The top panels show the wind-stress curl, which is the primary driver of the cross-shelf overturning circulation.

Considering that the shelf is particularly narrow in this region, high resolution in both the atmosphere and the ocean is required to properly represent this dynamics. This cross-shelf overturning circulation is seasonally enhanced, in particular in summer in the Central Region (Figure 2e), while in the Northern Region a sign reversal in wind stress curl strengthens the downwelling cell in winter (Figure 2c).

The strong positive wind-stress curl in summer favors the formation of an intense upwelling front on the inner shelf, which is balanced by a surface equatorward current on the Central and Northern Shelves (Figures 2e and 2f). The vertical shear is intense enough that the current reverses direction at depth, turning into a poleward coastal undercurrent, which in turn provides a source of baroclinic instabilities that foster eddy exchanges of heat, salt, and BGC materials between shelf and offshore waters (Colas et al., 2013; Marchesiello et al., 2003; Nagai et al., 2015).

Figure 2 reveals that the cross-shelf overturning comprises a bottom-confined transverse cell dominated by downward and offshore flow next to the seafloor. This cell is active throughout the whole year, and is generally shallower in winter, and deeper in summer. In the Southern and Central Regions, the downslope bottom flow is intensified during summer upwelling, whereas in the Northern Region it is greater during winter downwelling. As suggested by the correlation with the alongshore current, this cross-shelf circulation likely results from shear stress via Ekman dynamics in the bottom boundary layer. Generation of bottom shear on the deeper shelf were reported for the USWC (Lentz & Chapman, 2004; Perlin et al., 2005) and the NW Iberian continental shelf (Villacieros-Robineau et al., 2019). Here, we highlight the poleward California undercurrent as central in the generation of bottom shear, and the overlooked role of this bottom cell as an essential margin-to-open-ocean transport pathway that exports biogeochemical material offshore outside the surface euphotic layer.

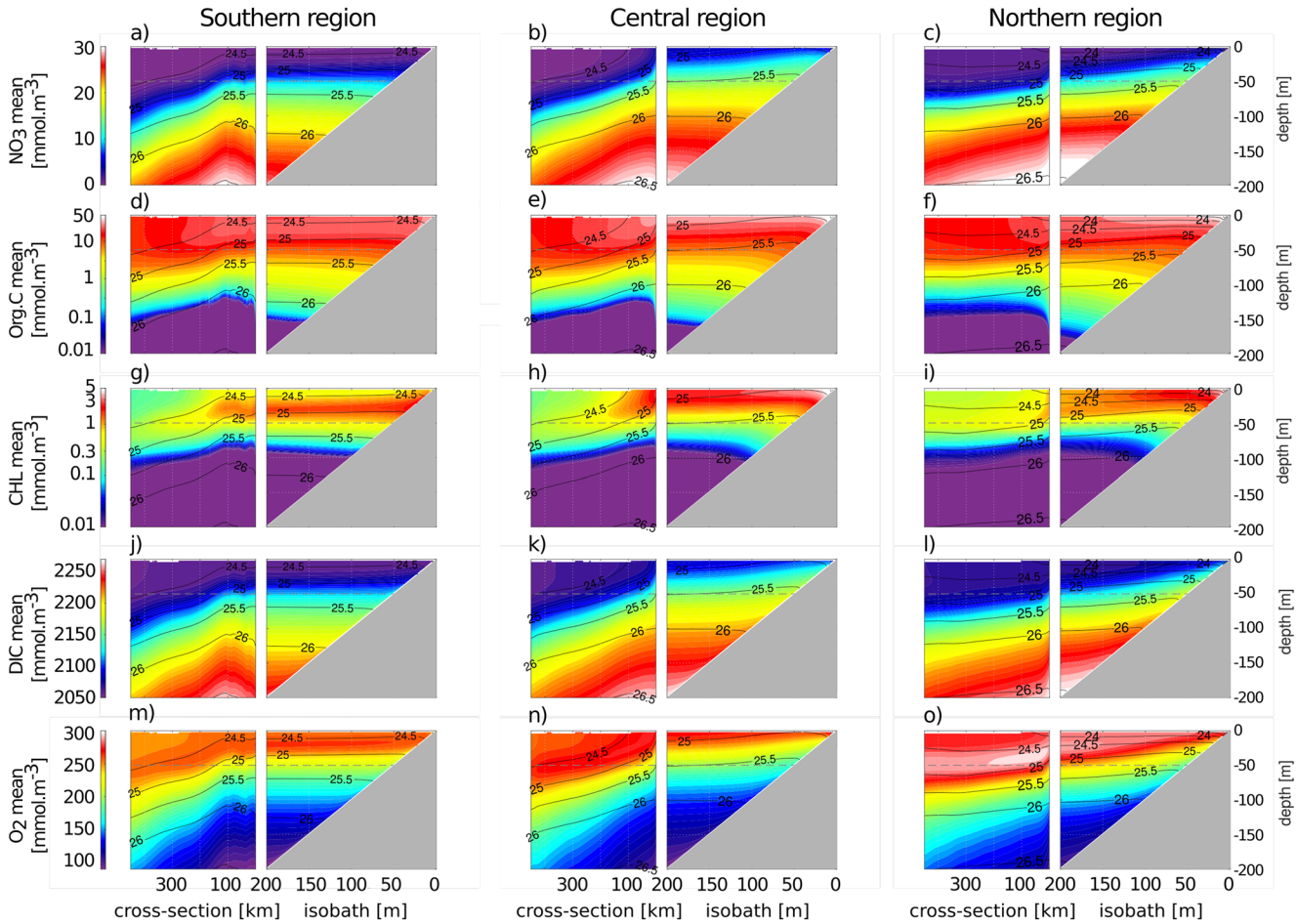

Figure 3. Vertical cross-shore sections of NO_3 (a, b, c), OC (d, e, f), chlorophyll (g, h, i), DIC (j, k, l), and O_2 (m, n, o) concentrations averaged in the (left) Southern, (center) Central, and (right) Northern Regions from December 1999 to November 2007. The dashed black contours show isopycnal surfaces with labeled potential density anomalies.

The complex wind-driven dynamics on the shelf leaves a clear imprint on BGC tracers (Figure 3). Nutrient- and DIC-rich and O_2-depleted waters are brought to the surface on the shelf, generating strong cross-shore BGC gradients, while in the euphotic layer organic biomass and chlorophyll decrease with the distance from the coast. These patterns can be observed coast-wide, and are particularly pronounced in the Central Region, in agreement with a variety of observations, for example, from CalCOFI (Bograd & Mantyla, 2005).

3.2. BGC Balances

The major BGC role of the shelf is reflected in the coast-wide balances of C, O_2, and N, shown in Figures 4 and 5. We focus on area- and time-averaged BGC rates integrated between 0 and 50 m depth, to highlight the intense cycling on the shelf, while reporting spatially integrated fluxes in Appendix C (Figures C1 and C2).

Offshore, primary production converts DIC to OC at a rate of 54.2×10^{-8} molC m^{-2} s^{-1} (10^{-8} mol m^{-2} s^{-1} = 0.864 mmol m^{-2} y^{-1}) (Figure 4). The majority of newly-formed organic matter (73%) is directly remineralized in the euphotic layer, with the remainder exported as sinking particles (18%) and by isopycnal eddy diffusion and advection (9%). On the shelf, carbon assimilation is about twice as large as offshore (113.5×10^{-8} molC m^{-2} s^{-1}). Approximately 52% of the organic matter is remineralized in the euphotic layer, 22.5% is exported as particles below the euphotic layer or into the inner-shelf sediment, and 25.5% by lateral advection. Similar to assimilation, particle export and remineralization nearly double on the shelf compared to offshore, whereas atmospheric CO_2 uptake occurs at comparable mean rates. On the shelf, the outgassing of excess CO_2 in recently upwelled DIC-rich waters in central California (consistently with Laruelle et al. (2014) and Turi et al. (2014)) is

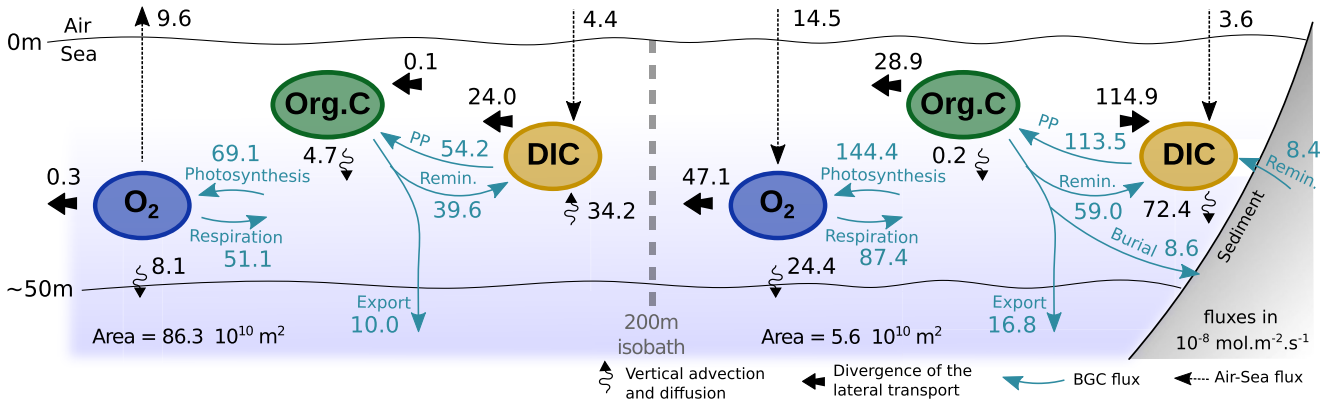

Figure 4. Area-normalized, upper-ocean mean carbon and oxygen cycle balances along the U.S. West Coast. Units are 10^{-8} mol m^{-2} s^{-1}. The colored circles represent biogeochemical tracers resolved by the model (Org. C = organic carbon; DIC = dissolved inorganic carbon), the thin blue arrows biogeochemical transformation rates, and the thick black arrows net lateral transport. Transport terms are calculated as the divergence of horizontal advective fluxes, and correspond to the local time rate of change solely due to the horizontal circulation. Arrows directed toward a tracer represent positive terms in the tracer balance, that is, sources, and arrows directed away from it represent negative terms, that is, sinks. The corresponding area-integrated fluxes are shown in Figure C1 in Appendix C.

overwhelmed by the substantial CO_2 uptake by photosynthesis in the Southern and Northern Regions (see Appendix D for further details on air-sea fluxes).

The intensification of BGC rates on the shelf arises from contrasting patterns of nutrient supply to the euphotic layer (Figure 5). Offshore, N delivery occurs nearly exclusively as nitrate (~95%), by a combination of isopycnal diffusion and lateral advection. This transport feeds new primary production at a rate of 2.0×10^{-8} molN m^{-2} s^{-1}, and it is balanced by export of organic matter primarily as sinking particles (by about 70%). As a consequence, ammonium regeneration tightly balances ammonium uptake (5.4×10^{-8} molN m^{-2} s^{-1}), resulting in low nitrification rates, and an *f–ratio*, here defined as nitrate uptake over total primary production, of 0.27.

Because of wind-driven overturning, the surface nitrate supply by advection and diffusion on the shelf is about 3.4 times higher than offshore, driving an average assimilation rate of 6.6×10^{-8} molN m^{-2} s^{-1}. Note that, on the shelf, nitrification is a non-negligible source of nitrate (~10%). Because of nitrification, ammonium release (of which ~13% from the sediment) is not fully balanced by ammonium uptake (8.8×10^{-8} molN m^{-2} s^{-1}), and the *f–ratio* is larger on the shelf (~0.43) than offshore. Of the organic nitrogen (ON) produced on the shelf, 52% is remineralized, 23% is exported by settling particles, and 25% by lateral advection away from the shelf.

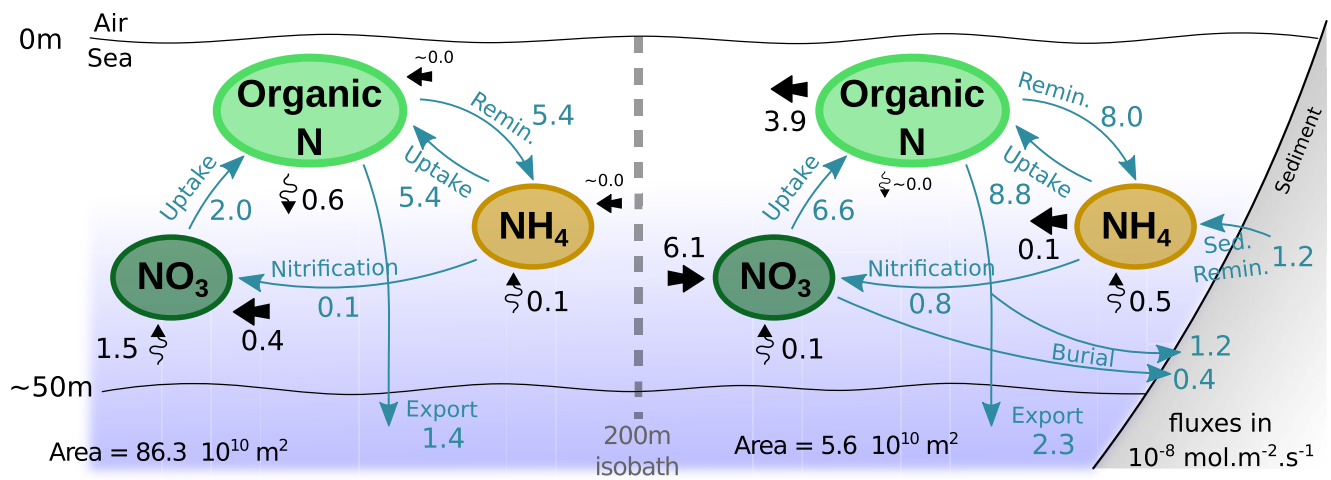

Figure 5. Area-normalized, upper-ocean nitrogen cycle balance along the whole U.S. West Coast. See caption of Figure 4 for additional details. The corresponding area-integrated fluxes are shown in Figure C2 in Appendix C.

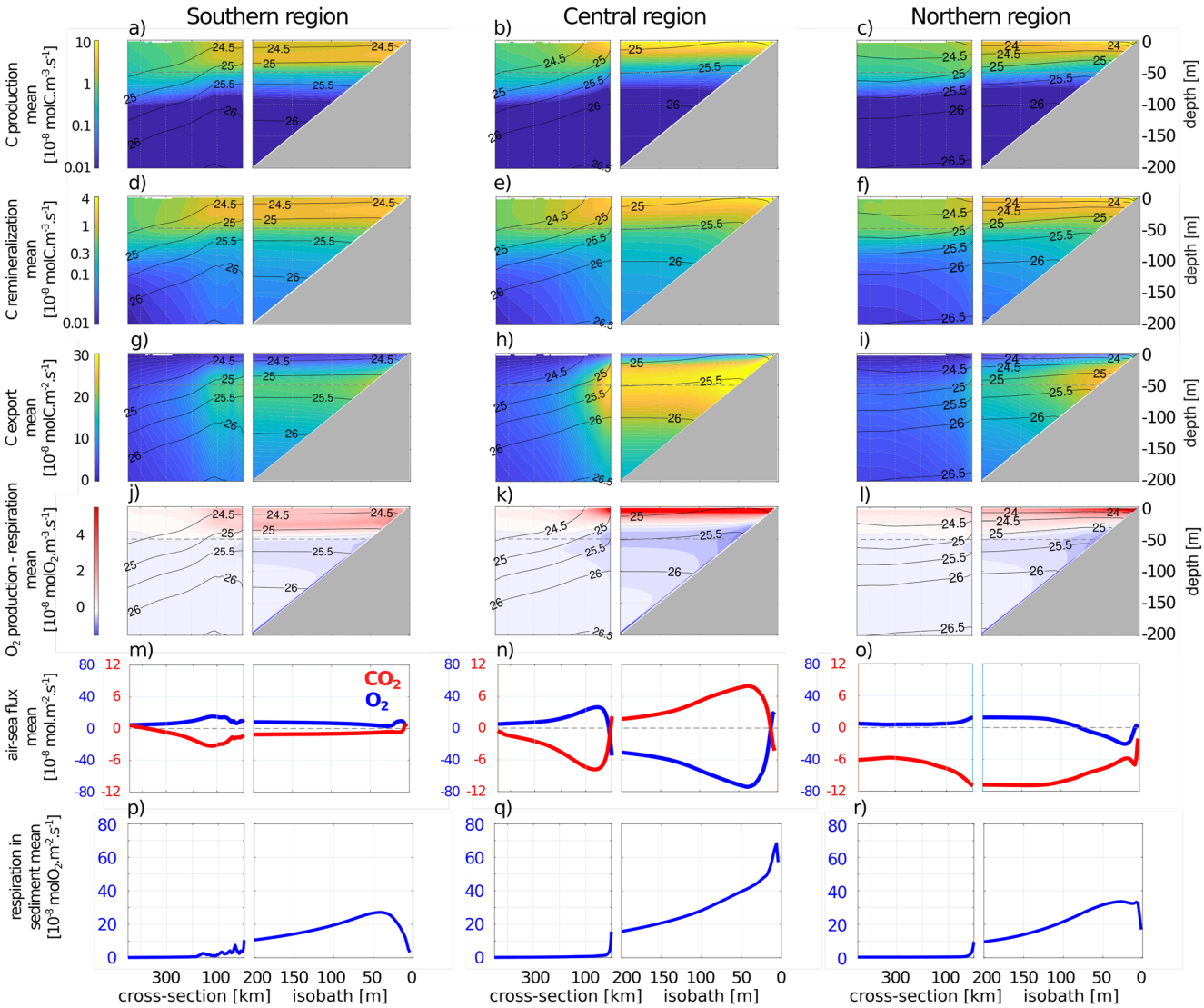

Figure 6. Vertical cross-shore sections of primary production (a, b, c in molC m^{-3} s^{-1}), carbon remineralization (d, e, f in molC m^{-3} s^{-1}), particulate flux (g, h, i in molC m^{-2} s^{-1}), oxygen production minus respiration (j, k, l in $molO_2$ m^{-3} s^{-1}), air-sea fluxes (m, n, o, in molC m^{-2} s^{-1}) of CO_2 (red) and O_2 (blue), with positive values out of the ocean, and negative values into the ocean, and respiration in the sediment (p, q, r in $molO_2$ m^{-2} s^{-1}), averaged in the (left) Southern, (center) Central, and (right) Northern Regions from December 1999 to November 2007. The dashed black contours show isopycnal surfaces with labeled potential density anomalies.

Production of O_2 by photosynthesis and consumption by respiration are about twice as large on the shelf as offshore (respectively by a factor of 2.1 and 1.7). Note that O_2 produced in the sunlit zone of the shelf also ventilates deeper layers, and is laterally exported toward the open ocean.

In addition to this cross-shore variability, BGC rates are characterized by strong vertical gradients and along-shore variability between the three USWC regions (Figure 6). Net community production mainly occurs in the uppermost 50 m of the water column, and it sharply decreases to negligible rates at depth. Similarly, about 70% of the vertically integrated remineralization occurs in the 0–50 layer , although substantial rates are observed at depth, mostly driven by organic particle decomposition. Sinking particle fluxes reach a maximum at about 50 m (Figures 6g–6i), coinciding with the phytoplankton compensation depth, where respiration equals photosynthesis.

On the shelf, significant particulate organic carbon fluxes reach the sea floor at depths shallower than 100 m, where they drive intense benthic respiration (Figures 6p–6r), release of DIC at the sediment-water interface, and, carbon burial into coastal sediment. The cross-shore variation in sedimentary respiration is noteworthy, because

it is a primary source of low-oxygen and low-pH conditions that impact coastal benthic ecosystems (Fennel & Testa, 2019).

While BGC rates show similar spatial patterns in the three USWC regions, they display significant variability. For instance, BGC rates are higher in the Central Region, where primary production can exceed 25×10^{-8} molC m^{-3} s^{-1} at the surface, and lower in the Southern Region, where their vertical gradients are also weaker.

Air-sea fluxes contrast with other BGC rates by their particularly pronounced spatial variability (Figures 6m–6o). Due to high DIC concentrations, the central shelf experiences large CO_2 outgassing (with maximum annual rates along the 40 m isobath), while ingassing dominates on the northern and southern shelves. The magnitude of the CO_2 flux increases with latitude: the annual ingassing of CO_2 is larger in the Northern Region, reaching up to 10.9×10^{-8} molC m^{-2} s^{-1} on the outer shelf, whereas it does not exceed 3.3×10^{-8} molC m^{-2} s^{-1} in the Southern Region. A local peak in CO_2 outgassing in the Southern Region is associated with the Channel Islands, where recurrent cyclonic eddies expose subsurface waters to the atmosphere. These patterns are broadly consistent with prior data-based assessments (Dai et al., 2022; Landschützer et al., 2020; Laruelle et al., 2014) and modeling studies (Fiechter et al., 2014), and provide a detailed picture of the underlying flux dynamics.

O_2 fluxes are largely anti-correlated with CO_2 fluxes, with ingassing dominating in the central shelf, and weak outgassing dominating in the southern and northern shelves. In the very nearshore region, a sign reversal in air-sea fluxes is often observed, a feature matched by in-situ measurements, for example, along CalCOFI line 77 (Fiechter et al., 2014), and likely driven by increased production very close to the coast.

In summary, the largest BGC rates on the USWC are found on the shelf, sustained by the vigorous upwelling-driven overturning circulation, and they rapidly decrease offshore. For completeness, we include several Appendices describing the BGC temporal variability (Appendix B), a detailed USWC budget analysis (Appendix C), the seasonal variability in air-sea fluxes (Appendix D), and a comparison of BGC rates with prior studies (Appendix E). In the next sections, we investigate how this enhanced shelf activity affects offshore BGC balances via lateral transport and tracer redistribution.

4. BGC Transport and Cycling on the Shelf

4.1. Carbon

Figure 7 shows the time-mean carbon transport and cycling rates on the three regions of the USWC continental shelf, integrated horizontally and from the surface to the bottom. As a whole, the USWC shelf represents a site of enhanced carbon assimilation that converts DIC to OC at an average rate of (14.1×10^3 molC s^{-1}), before exporting it at a rate of 14.4×10^3 molC s^{-1}, with a small residual (0.3×10^3 molC s^{-1}) accounted for OC terrestrial inputs from the Juan de Fuca Strait and sediment deposition. Of the total OC export from the USWC shelf, 90% occurs across the continental slope, rather than meridionally. Along-shore transport across the northern and southern boundaries account for 8% and 2% of the OC export respectively.

In contrast, there are large lateral fluxes and recirculation of DIC across shelf boundaries, with significant import from offshore to the Southern and Northern Regions, and significant export offshore from the Central Region, and along-shore from the Northern Region. Overall, the net supply of DIC occurs mainly across the continental slope, with a net input of 163.1×10^3 molC s^{-1}.

Because of intense upwelling, more than half (63.1%) of the net biological carbon assimilation occurs in the Central Region, which also contributes by about three quarters (78.3%) to the cross-shelf OC export to the open ocean. The lack of balance between OC production and export results mainly from the meridional convergence of DIC and OC fluxes that increase the local carbon content, promoting export of DIC and OC offshore, and release of CO_2 to the atmosphere. The Southern and Northern Regions contribute respectively 7.8% and 29.1% of the net carbon assimilation, and 1.5% and 20.2% of the OC offshore export.

Air-sea and sedimentary C fluxes are an order of magnitude smaller than lateral transport, accounting for ∼14% and ∼1% of the net DIC input to the shelf, respectively. Terrestrial sources, here represented by exchange through the Juan de Fuca Strait, which connects the USWC to the Salish Sea at the U.S. northern border, are not negligible (∼25% of the total DIC input in the northern region).

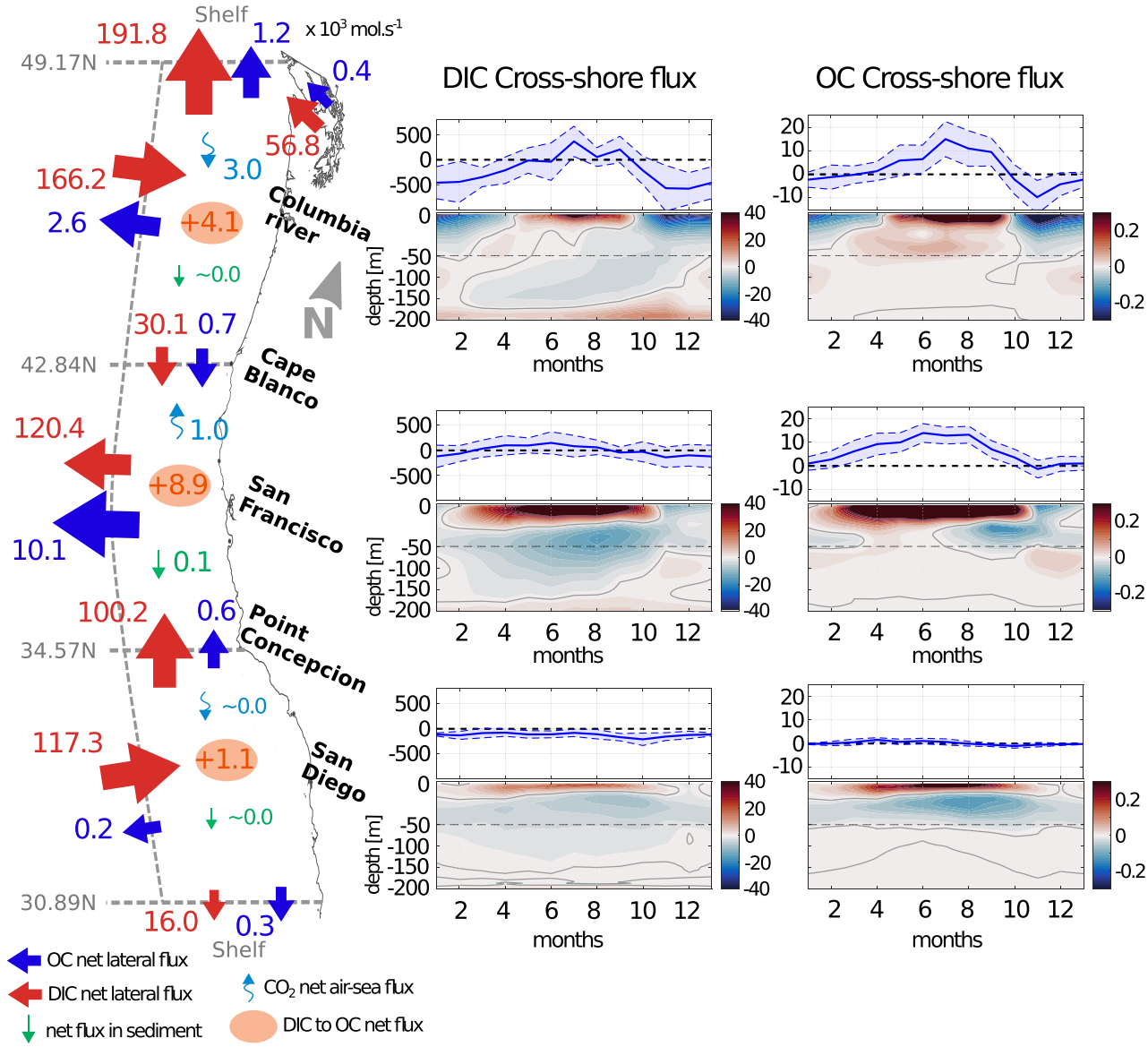

Figure 7. (Left column) Carbon transport and cycling on the USWC shelf (in 10^3 molC s^{-1}). (central column) DIC and (right column) OC monthly flux across the 200 m isobath integrated over the (upper) northern, (middle) central, and (bottom panels) southern regions. Each panel displays the (upper panels) flux integrated over the vertical (in 10^3 molC s^{-1}) as solid blue lines with one standard deviation shown by the shading, and the (lower panels) vertical profiles (in 10^{-3} molC m^{-2} s^{-1}) shown as color shading.

Figure 7 also shows the vertical structure and seasonal variability of the cross-shelf exchange of DIC across the 200 m isobath. Both are strongly influenced by the cross-shelf overturning circulation shown in Figure 2. During upwelling, DIC is transported into the shelf in the water column interior (Figure 7, central column), that is, outside the surface and bottom boundary layers. Export of DIC from the shelf to the open ocean occurs instead within these boundary layers. During winter downwelling in the Northern Region, transport reverses direction at the surface and in the interior, while it remains offshore at the bottom.

The bulk of OC exchange between the continental shelf and the offshore region takes place in the upper Ekman layer, reflecting strong surface currents and high OC concentration. In the Southern Region, the cross-shelf export remains low (<2.0×10^3 molC s^{-1}) due to a partial compensation between offshore transport above 20 m and inshore transport below it. The total offshore transport from the Central Region reaches up to 14.0×10^3 molC s^{-1} at the beginning of upwelling, driven by increasing offshore OC transport at the surface (from 0.08×10^{-3} molC m^{-2} s^{-1} in February to 1.01×10^{-3} molC m^{-2} s^{-1} in June). After June, as organic matter

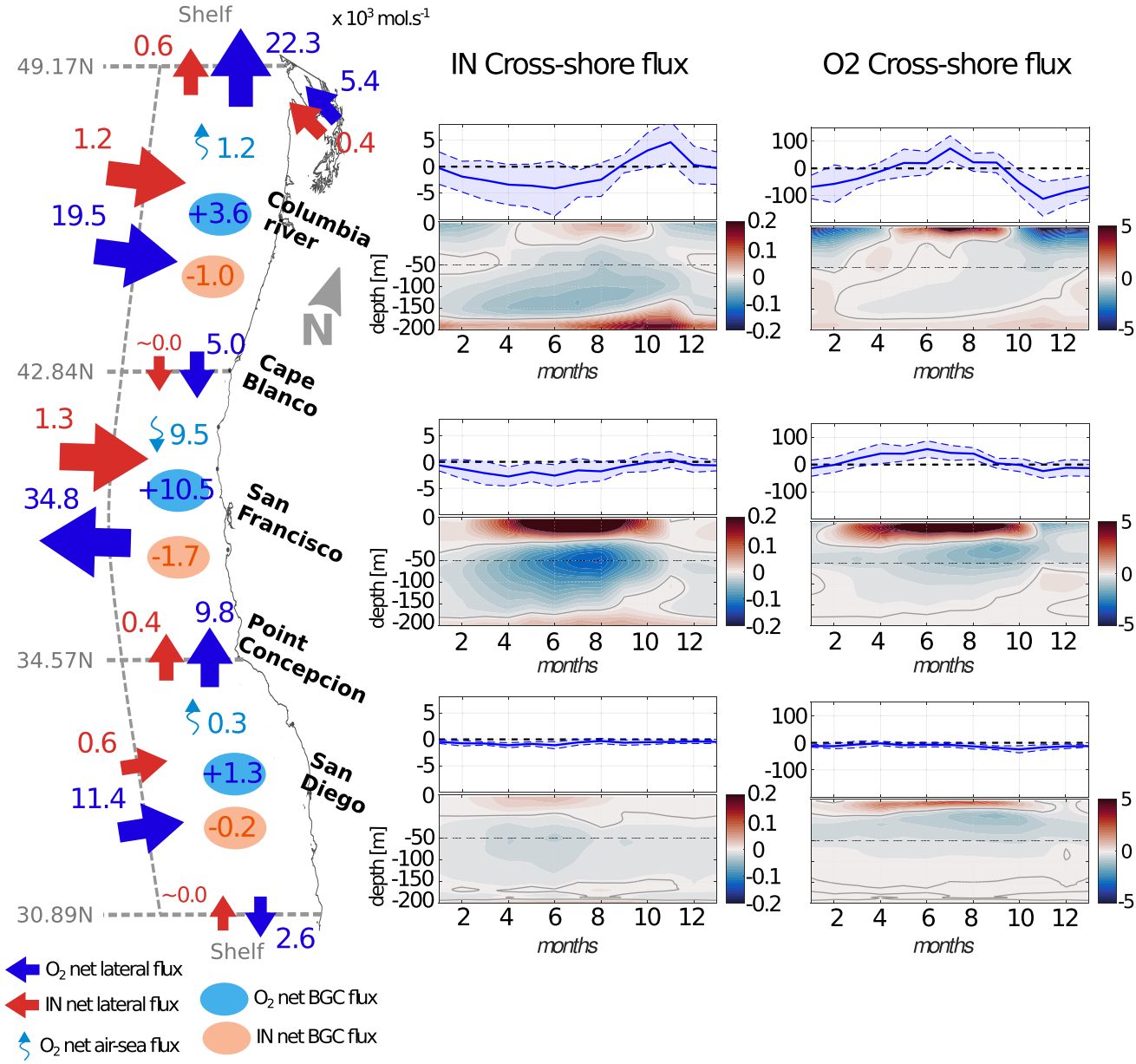

Figure 8. Same as Figure 7 for inorganic nitrogen and oxygen.

accumulates offshore, inshore transport of OC increases, first in subsurface layers from July to October, then from the whole euphotic layer until December. The inshore flux reduces the net OC export from the shelf during upwelling (July and August).

4.2. Inorganic Nitrogen

The USWC continental shelf acts as a net sink of inorganic nitrogen (~2.9×10^3 molN s^{-1}; Figure 8). Biological IN assimilation is largely balanced by the net IN transport across the shelf break (3.1×10^3 molN s^{-1}). This first-order IN balance is closed by a net terrestrial input in the Northern Region (0.4×10^3 molN s^{-1}), and net export across its northern boundary (~0.6×10^3 molN s^{-1}). Cross-shore transport is maximum in the Central Region, reflecting the strong upwelling (1.3×10^3 molN s^{-1}). Along-shore transport is significant at Point Conception, where a net IN supply by the northward coastal counter-current fertilizes the central coast. The significant IN inputs from southern waters is consistent with the results Frischknecht et al. (2018).

The net cross-shelf IN transport results from a balance between inshore and offshore fluxes with a characteristic vertical structure and seasonal cycle (Figure 8 central column). In the Southern and Central Regions, the cross-shelf transport closely reflects the upwelling-driven overturning (Figure 2), which transports IN inshore at depth, and offshore in the surface boundary layer. Similar to the upwelling intensity, cross-shore fluxes are much lower in the Southern Region compared to the Central Region, where inshore transport can reach up to 0.13×10^{-3} molN m^{-2} s^{-1} at about 50 m depth, and offshore fluxes up to 0.43×10^{-3} molN m^{-2} s^{-1} at the surface. Bottom Ekman layer dynamics drives substantial offshore IN export year-round in the Central Region. Integrated over the first 20 m above the sea floor, it exports 0.3×10^3 molN s^{-1} on average, with a maximum of 0.6×10^3 molN s^{-1} during peak upwelling.

Seasonal variability in cross-shelf IN transport is particularly pronounced in the Northern Region. Net inshore fluxes are higher in summer, during upwelling. From October to April, downwelling drives offshore transport at about 50 m depth, and inshore transport at the surface. Export by the bottom boundary layer is considerable (2.0×10^3 molN s^{-1} in average), reaching up to 4.0×10^3 molN s^{-1} during October and November, when it dominates the net cross-shelf exchange.

4.3. Oxygen

As a result of intense photosynthesis, the USWC shelf is a location of net O_2 production (15.4×10^3 molO_2 s^{-1} of which ~68.2% occurs in the Central Region; see Figure 8). The O_2 circulation resembles DIC transport, except for air-sea fluxes, which have opposite patterns. Indeed, despite strong production (Figures 4 and 5), the USWC shelf is a site of net O_2 ingassing, mainly occurring in the Central Region.

Wind-driven overturning exposes low-O_2 waters to the surface, where they are replenished by gas exchange and photosynthesis. On the shelf, newly-produced O_2 is exported offshore in the surface Ekman layer, while the northern and southern shelf boundaries, as well as the bottom boundary layer, constitute secondary pathways of O_2 export. In particular, the bottom Ekman layer, with an average offshore flux of 10.0×10^3 molO_2 s^{-1}, represents an overlooked pathway for ventilating O_2-poor waters along the deeper parts of the USWC shelf.

Similar to those of DIC, along-shore O_2 fluxes represent an important component of the O_2 balance on the shelf. Their convergence in the Central Region provides the largest source of O_2 (14.8×10^3 molO_2 s^{-1}), exceeding net biological O_2 production. In contrast, in the Southern and Northern Regions, O_2 export in the along-shore direction represents a O_2 source for the adjacent Baja California and Canadian shelves.

4.4. Cross-Shore Eddy Fluxes

The lateral transports shown in Figures 7 and 8 arise from a combination of mean and eddy fluxes, the latter of which are particularly vigorous in the region (Capet et al., 2008; Dauhajre et al., 2017; Gruber et al., 2011; Kessouri, Bianchi, et al., 2020). Figure 9 shows the mean and eddy BGC fluxes across the shelf break and their vertical structure, highlighting three main exchange pathways: the surface and bottom boundary layers, confined to the top and bottom 20 m, and an interior route in the intermediate layer.

The offshore surface boundary layer transport in the Southern and Central Regions (Figures 9a and 9b) results from the combination of mean and eddy offshore fluxes, with the magnitudes of eddy-fluxes comparable in the two regions. In the Southern California Bight (Figure 9a), both components have similar magnitudes, while eddy-driven fluxes are smaller than mean fluxes in the Central Region (Figure 9b). This is due to the much more intense mean transports in the Central Region that overwhelm eddy components. This is particularly true for OC transport (Figure 9.b.2). In this region, the stronger effect of surface eddy fluxes on IN (Figure 9.b.1) as compared to OC (Figure 9.b.2) and O_2 (Figure 9.b.3) indicates that eddies efficiently export upwelled nutrients offshore before they get completely assimilated. While expected, this high level of eddy-induced transport is lower than prior estimates (Gruber et al., 2011; Nagai et al., 2015), partly because of the smaller scales investigated here, and the focus on the nearshore region. The surface boundary layer transport differs in the Northern Region (Figure 9c). The wintertime surface coastal convergence is balanced by summertime surface coastal divergence for IN eddy and mean transports (Figure 9.c.1), resulting in a negligible annual mean net transport. The balance is dominated by onshore mean downwelling for O_2 and DIC (Figures 4 and 9.c.3, note the large vari-

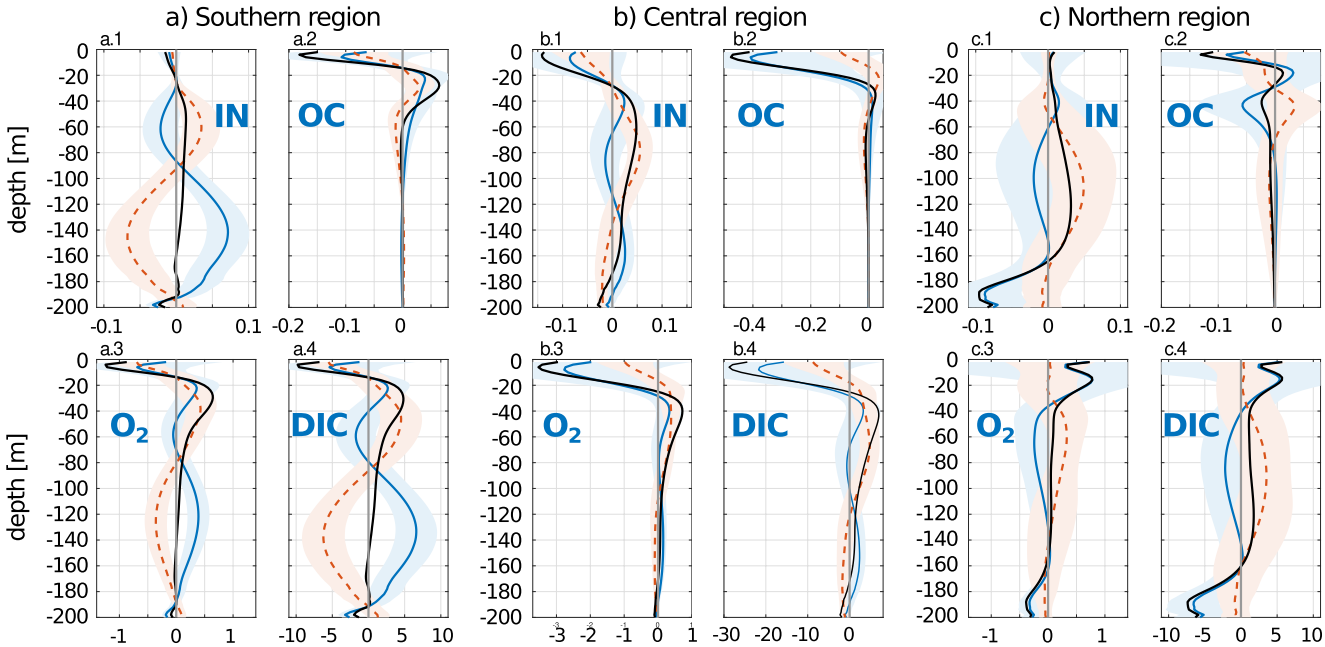

Figure 9. Total (solid black line), mean (solid blue line), and eddy (dashed red line) lateral biogeochemical fluxes across the 200 m isobath (in 10^{-3} mol m^{-2} s^{-1}). Shaded envelopes indicate the monthly variability (1 s.d.) of the mean and eddy components. Positive fluxes are directed inshore. Note the different scale on the *x*-axis for the Central Region. The gray solid line shows 0 cross-shore flux.

ability associated), with a seasonal compensation of eddy fluxes. Driven by high primary production during the upwelling season, the surface boundary layer OC mean and eddy transports are directed offshore.

In the intermediate layers, the onshore transport is characterized by a significant anticorrelation between mean and eddy fluxes. The eddy terms largely oppose the mean terms, with similar contributions in the Southern and Northern Regions (Figures 9a and 9c), and a dominant contribution in the Central Region. In particular, eddies transport inorganic nutrients into the shelf in the 90–40 m layer of the Southern Region, and through the intermediate layer of the Central and Northern Regions. This role for fine scale circulation in transporting nutrients and other material on-shelf differs from previous works (Gruber et al., 2011; Nagai et al., 2015). This can be partly explained by the explicit focus on the shelf of this study. In addition, a critical feature of the offshore transport classically attributed to eddy transport in the CCS is the sharpening of the upwelling front, which causes convergence and subduction of organic matter and nutrients. This front is typically found between 30 and 60 km offshore (Nagai et al., 2015), that is, outside the shelf in our model (Figure 1). Thus, part of the material subducted along the upwelling front is likely advected back onto the shelf by eddies. This idea is supported by the inshore eddy flux of organic matter between 50 and 20 m depth (Figure 9.b.2).

The bottom boundary layer transport provides a shelf-to-ocean export pathway that is particularly relevant in the Northern Region. The large, bottom-confined mean transport points to an active bottom boundary layer dynamics throughout the year. Eddy transport at the bottom might, at least partly, be driven by cross-shore meanders in the California undercurrent, or even by episodes in which the undercurrent detaches from the shelf to release submesoscale coherent vortices (Frenger et al., 2018; McCoy et al., 2020; Molemaker et al., 2015). The nearshore localization of the undercurrent south of Point Conception (Figure 2) may help explain the large eddy transport extending largely above the bottom, in the Southern Region (Figure 9a).

5. Discussion

Our study shows that, along the USWC, the largest BGC rates occur on the shelf, driven by the vigorous cross-shelf overturning circulation that results from wind-driven coastal upwelling/downwelling, Ekman pumping driven by the wind stress curl, and bottom boundary layer dynamics.

While continental margins represent only 6.0% of the total USWC area (considering an offshore limit at 400 km from the coast) our simulations show that they account for about 18% of the net IN flux to the euphotic zone, 14.3% of the total biomass, 11.9% of primary production, and 17.9% of new primary production. These results are consistent with studies suggesting that about 10%–15% of global primary production occurs on continental margins (Muller-Karger et al., 2005).

In addition to locally enhanced BGC rates, due to intense cross-shelf exchanges, the USWC shelf actively participates in the BGC dynamics of the open ocean. A large portion (~20.5%) of the organic matter produced on the shelf is exported toward the Pacific Ocean, comparable to a previous estimate of about 36% from Frischknecht et al. (2018). This export corresponds to about 10% of the net community production (i.e., net primary production minus remineralization) offshore. In other words, 10% of the organic matter found offshore is produced on the USWC shelf. Even if the net cross-shelf IN transport is directed inshore, the surface boundary layer represents a major pathway of IN export offshore. Integrated over the euphotic zone, the IN flux from the shelf to the open ocean equals 12.9% of the total nitrate supply to the euphotic layer offshore. This outgoing flux indicates that the time-scales for nutrient utilization on the shelf are too slow to allow complete drawdown of recently upwelled nitrate on the shelf, despite recent high-resolution estimates of enhanced water residence times on continental margins (Liu et al., 2019). Earlier estimates from Liu et al. (2010) and Frischknecht et al. (2018) were significantly larger, at respectively about 24% and 17%, perhaps reflecting the coarser resolution of those studies.

Our study also highlights the importance of the mean bottom boundary layer circulation, that is, the lower limb of the cross-shelf overturning, for shelf biogeochemistry. Transport in the bottom boundary layer drives a year-round offshore and downward flux of DIC, IN, and O_2 across the shelf break along the entire USWC shelf. This flux is substantial, and often of the same magnitude as the vertically integrated net transport. Its consequences for the chemical environment include removal of nutrients and DIC, ventilation of intermediate and deep parts of the shelf, and transport of low-O_2 waters downstream of seasonally anoxic shallow shelf sediment, as observed along the Oregon coast (Chan et al., 2008). Export of DIC and IN along the bottom partially counteracts mid-water transport onto the shelf, potentially reducing the productivity and water acidity of shallower layers. Tracer transport and transformation in the bottom boundary layer also set the properties of submesoscale coherent vortices that are spawned by the poleward undercurrent (Garfield et al., 1999; McCoy et al., 2020; Molemaker et al., 2015), in turn affecting subsurface biogeochemistry in the ocean interior (Frenger et al., 2018).

The important role of lateral transport of organic matter supports the idea of a fully three-dimensional biological pump along the continental margin of the USWC, as suggested by previous work (Frischknecht et al., 2018; Lovecchio et al., 2017). Our results give particular emphasis to the shelf (within the first 25 km of the shoreline on average) for the production and transport of organic matter to the open ocean, and its sequestration to deeper layers and the sediment. Yet, we downplay the classical view of eddy-driven transport as primarily an offshore flux followed by subduction into the subtropical gyre. On the shelf, our findings indicate an horizontal onshore eddy transport in the intermediate layer, with potential recirculation of material subducted along the upwelling front, painting a more complex view of the eddy-induced component of the biological pump (Lovecchio et al., 2017, 2018). The ability to resolve submesoscale eddies is likely important to correctly represent transport of organic matter and inorganic nutrients, as compared to mesoscale-resolving studies (Frischknecht et al., 2018; Kessouri, Bianchi, et al., 2020; Liu et al., 2010).

Considering a depth horizon of 200 m (or the sea floor for depths shallower than 200 m), we estimate an export flux of particulate organic carbon of 25.59 $TgCyr^{-1}$ for the USWC, of which 4.59 $TgCyr^{-1}$, that is, 17.9% of the total, over the shelf (i.e., to the sediment) (Table 1). Furthermore, 62.6% of the total flux of particulate organic matter to the sediment along the USWC takes place on the shelf. Thus, despite partial decoupling of carbon export from production on the shelf, coastal sediments are likely major actors in the long-term storage of carbon along the USWC margin, consistent with the global-scale estimate (>40%) from Muller-Karger et al. (2005).

Vigorous CO_2 outgassing in the Central Region is more than compensated by ingassing in the Northern Region, making the USWC shelf a relatively weak sink for atmospheric CO_2, with a net uptake of ~15.3 TgC yr^{-1} (Table 1), in agreement with the 14 (±14) TgC yr^{-1} from Hales et al. (2012) estimated over a similar region. Because this net flux is a small residual of large regionally-variable fluxes, even small errors in the representation of gas exchange or interpolation from undersampled datasets could lead to biased estimates of the importance of the USWC as an atmospheric CO_2 sink. Coupled to large seasonal variability (detailed in Appendix D), this likely explains the diversity of estimates for CO_2 fluxes that often consider slightly different regions (see Appendix E).

Table 1
Summary of the Main Carbon Cycle Fluxes Along the USWC (TgC yr^{-1})

	USWC	Shelf	Ratio (Shelf/USWC)
CO_2 air-sea flux	15.10	0.76	5.0%
Primary Production	200.61	23.84	11.9%
Particulate organic carbon flux at 200 m or shallower	18.26	4.59	25.1%
Flux directly to sediment	7.33	4.59	62.6%

Note. The units adopted here are commonly used in global carbon flux estimates, and allow comparisons between different studies. See Table E1 for a comparison of these fluxes with published estimates.

Following the atmospheric CO_2 increase caused by human emissions, uptake of atmospheric CO_2 along the UWSC and its transport into the ocean interior will continue to evolve toward a larger net CO_2 sink (Lacroix, Ilyina, Mathis, et al., 2021; Laruelle et al., 2018; Regnier et al., 2022). However, the extent and pace of this change remain unclear, because of the variety of mechanisms involved and the significant variability and non-linearity of the system. High resolution regional simulations are thus essential to shed light on future USWC uptake, storage, and transport of anthropogenic CO_2 (Dai et al., 2022).

While terrestrial inputs are generally important along continental margins, in this study we only represent inputs of biogeochemical material from the Juan de Fuca Strait, which largely dominates the total terrestrial discharge along the USWC (Hickey & Banas, 2008). However, additional river fluxes (mainly via the Columbia River and the Golden Gate Strait) and local anthropogenic inputs, for example, from agricultural and urban sources (Kessouri et al., 2021; Sutula et al., 2021), are likely to be locally important. We leave assessment of the role of these inputs to future studies.

6. Conclusions

In summary, due to the vigorous wind-driven overturning circulation (Figure 2) and specifically its curl-driven Ekman pumping component, the USWC shelf can be schematically represented as the BGC "engine" of the USWC. Figure 10 summarizes this picture, highlighting the bottom boundary layer as a novel export pathway for biogeochemical material.

By quantifying the balances of N, C, and O_2 and providing a consistent picture of the underlying processes, this study is a step forward for assessing the state of the coastal USWC biogeochemistry. Although predicting the future of coastal biogeochemistry under changing forcings is a complex undertaking (Howard et al., 2020;

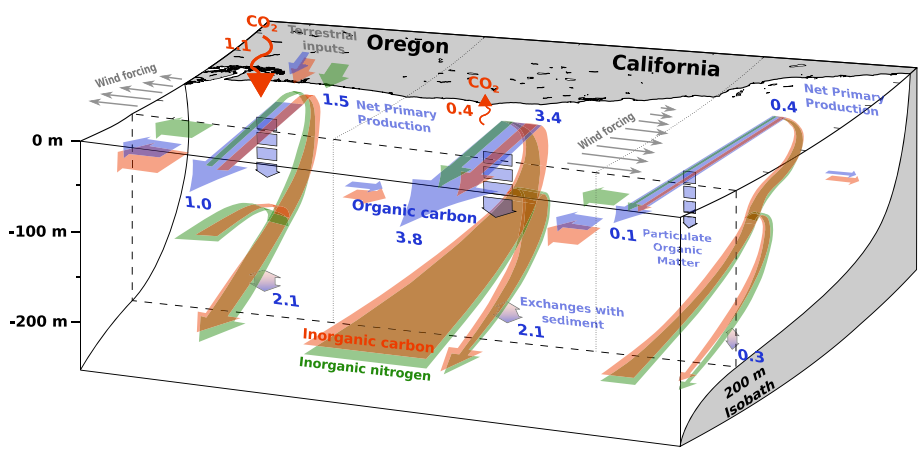

Figure 10. Schematic of carbon and nitrogen fluxes along the USWC and their drivers. Solid arrows show transport of organic carbon (blue), inorganic carbon (red) and inorganic nitrogen (green). Major regionally integrated carbon fluxes are reported in units of TgC yr^{-1}.

Pozo Buil et al., 2021), our study lays the basis for elucidating the interplay of C, N, and O_2 cycles at regional to local scales, highlighting the major elements required, and providing a framework for studying variability and future trends.

In particular, our analysis highlights several new aspects of biogeochemistry along the USWC: (a) The presence of vigorous and highly fluctuating BGC fluxes on the shelf, approximately twice as large as offshore, which are largely under-sampled in observations, and under-resolved by current models; (b) The role of eddies that not only export nutrients and organic matter from the nearshore region, mostly near the surface, but also contribute to enriching the shelf via horizontal subsurface fluxes directed inshore; and (c) The importance of the bottom boundary layer circulation, which removes inorganic nutrients and DIC from the shelf by exporting them offshore, thus partially balancing sedimentary fluxes, and provides a O_2 ventilation mechanism for the outer shelf, thus mitigating hypoxia and acidification on the USWC margin.

The results shown in this paper are based on numerical methods that provide a realistic simulation of the coastal-open ocean continuum down to the submesoscale (McWilliams, 2016) and analysis in a novel coordinate system that emphasizes shelf processes. In the intense eddying regime associated with upwelling (Capet et al., 2008; Kessouri, Bianchi, et al., 2020; Lévy et al., 2018; Nagai et al., 2015), this requires a resolution fine enough to represent submesoscale currents that induce vigorous cross-shore exchange with a complex vertical structure (Figure 9). Because of the chaotic nature of the mesoscale and submesoscale regimes, solutions spanning a period of several years or longer are needed to produce statistically robust representations of biogeochemical balances along the shelf. The resolution used in this study, 1 km, and the duration of the simulations, 10 years, appear to be an effective compromise to achieve a detailed, robust representation of biogeochemical balances along the shelf. However, quantification of multi-decadal to longer trends would require even longer simulations (Deutsch et al., 2021).

Our study supports the idea that the importance of continental margins in global BGC cycles has likely been underestimated (Laruelle et al., 2018; Liu et al., 2010; Muller-Karger et al., 2005; Najjar et al., 2018). However, while we find significantly enhanced primary production and organic carbon sequestration into the sediment along the USWC shelf, CO_2 air sea-fluxes are not dramatically different than in the open ocean, reflecting compensation between upwelling of CO_2-rich waters and enhanced biological uptake. Lateral exchange of nutrients and organic matter between the shelf and the open ocean is also substantial, consistent with a three-dimensional biological pump along the continental margin (Frischknecht et al., 2018; Lovecchio et al., 2017). This exchange reflects a combination of transport pathways on the shelf, which includes eddies and bottom boundary layer circulation. Both remain significant sources of uncertainty for global estimates, with significant regional variability and compensating effects when vertically integrated.

While computational limitations prevent application of our numerical approach at the global scale, analysis of similar high-resolution regional configurations can help filling current knowledge gaps. Some of the general patterns that we simulate along the USWC likely apply to other Eastern Boundary Upwelling Systems with similar wind-driven circulation, for example, the role of eddies and bottom boundary layer transport on the shelf. However, the large spatial variability that we observe along the USWC also implies that extrapolation to other continental margins will be difficult, even for Eastern Boundary Upwelling Systems. The fine-scale nature of many of the processes that drive BGC cycles on continental shelves will likely require concerted high-resolution simulations grounded by local observational studies, in order to achieve robust global syntheses (Dai et al., 2022; Regnier et al., 2022).

Appendix A: USWC Dynamical Regions

Based on geographical, meteorological, and bathymetric characteristics, and the circulation dynamics, we separate the USWC into three main coherent regions, each one characterized by consistent patterns in atmospheric and oceanic variables (Figure A1).

- The *Southern Region* (blue-shaded area in Figure 1) is characterized by the complex topography and re-circulation of the Southern Californian Bight. Surface waters in the region are relatively warm and salty (Figure A1) due to advection of low-latitude waters by the Southern California Counter-Current. High surface

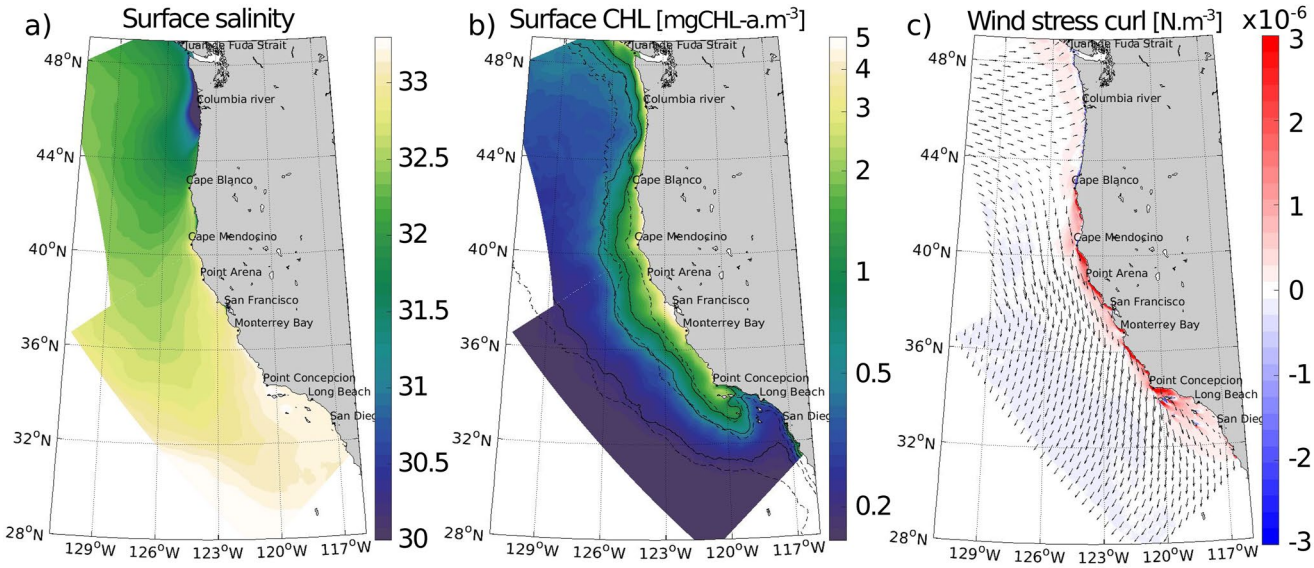

Figure A1. Maps of (a) surface salinity, (b) surface chlorophyll, and (c) wind stress curl in the USWC averaged from December 1999 to November 2007. Contours of 0.2, 0.5, and 1 mgChl m^{-3} for (full line) the solution and (dashed line) climatological MODIS-Aqua observations (Esaias et al., 1998) are superimposed on panel b. Black arrows represent the wind field at 10 m height.

chlorophyll concentrations are encountered around the islands and near the coast. Along-shore equatorward winds, with relatively weak seasonal variability, produce a year-long coastal upwelling of moderate intensity.

- The *Central Region* (red-shaded area in Figure 1) is characterized by intense coastal upwelling driven by strong along-shore winds in summer. The coastal wind drop-off generates an intense positive wind curl (Figure A1) that further strengthens upwelling (Renault, Hall, & McWilliams, 2016), with significant impacts on BGC (Messié et al., 2009; Renault, Deutsch, et al., 2016). The vigorous supply of nutrients supports high chlorophyll concentrations that extend 100s km offshore.
- Intense river fluxes and nutrient discharge affect the *Northern Region* (green-shaded area in Figure 1) extending northward to Vancouver Island (Hickey & Banas, 2008). Here, winds are mostly along-shore, but reverses direction from equatorward to poleward during winter. This drives coastal upwelling during summer, and coastal downwelling during winter. The continental shelf is wider in this region, with multiple canyons carving the continental slope.

This separation of the USWC into three coherent regions is overall consistent with previous work (Fiechter et al., 2018; Hales et al., 2012; Kämpf & Chapman, 2016; King et al., 2011; Renault, Hall, & McWilliams, 2016), although boundaries between regions, in particular between the Central and Northern ones, may differ between studies (Jacox et al., 2014). Here, we choose Cape Blanco as the separation because the climatological coastal wind stress curl is positive, and consequently upwelling-favorable, south of the Cape, whereas it is negative north of it (Figure A1).

The annual mean chlorophyll concentration at surface is in agreement with satellite observations (MODIS-Aqua). The main modeling mismatch occurs in the Northern Region probably due to the absence of an explicit river discharge in the model, especially the Columbia River (Banas et al., 2009).

Appendix B: Variability of BGC Quantities and Rates

As a complement to the mean BGC material distributions and rates in Figures 3 and 6, here we present daily and monthly variability maps, using a root-mean-square (RMS) measure for the fluctuations (Figures B1 and B2).

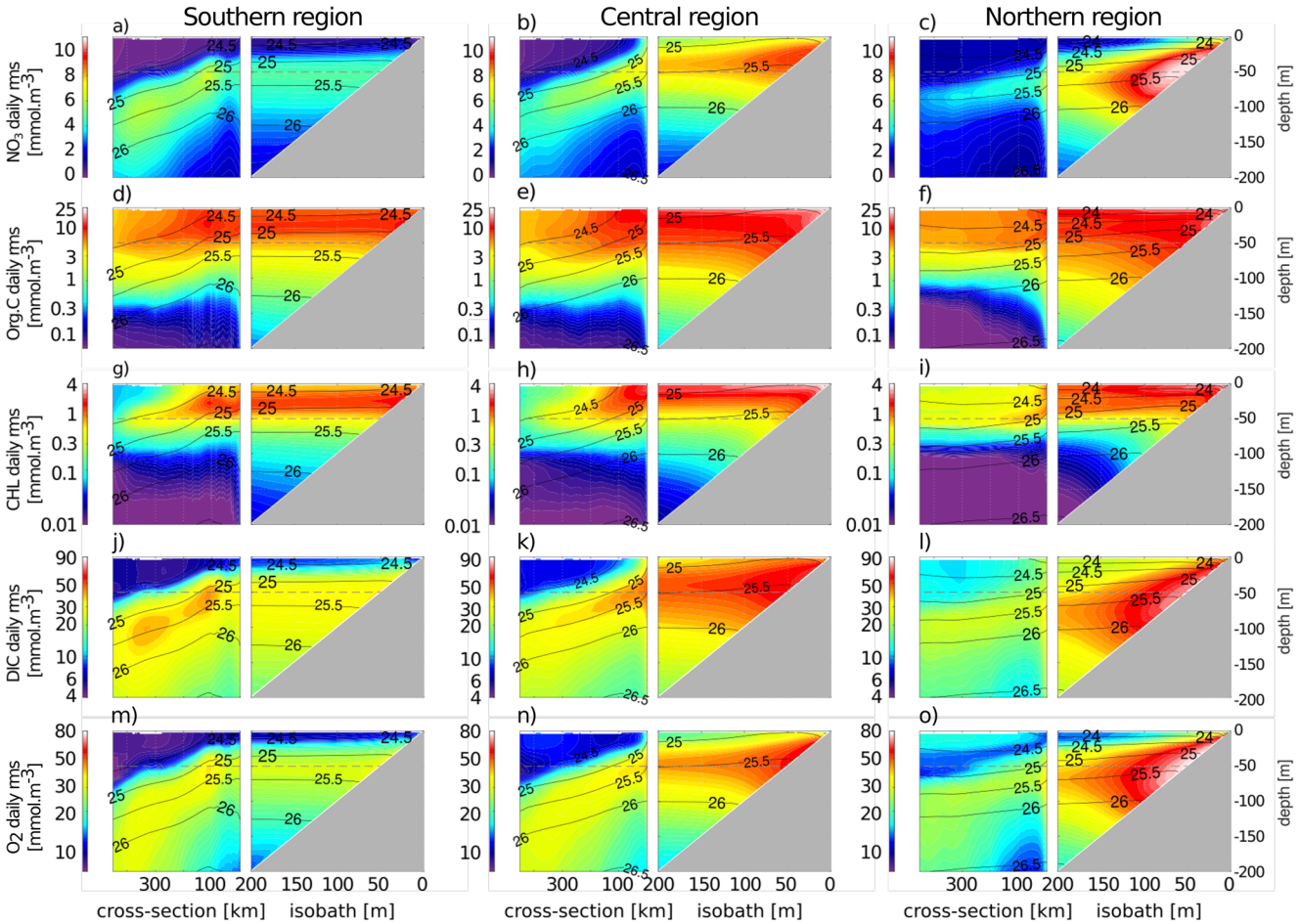

Figure B1. Vertical cross-shore sections of the daily RMS for (a, b, c) NO_3, (d, e, f) OC, (g, h, i) chlorophyll, (j, k, l) DIC, and (m, n, o) O_2 concentrations averaged in the (left) Southern, (center) Central, and (right) Northern Regions from December 1999 to November 2007. The dashed black contours represent isopycnal surfaces with labeled potential density anomalies.

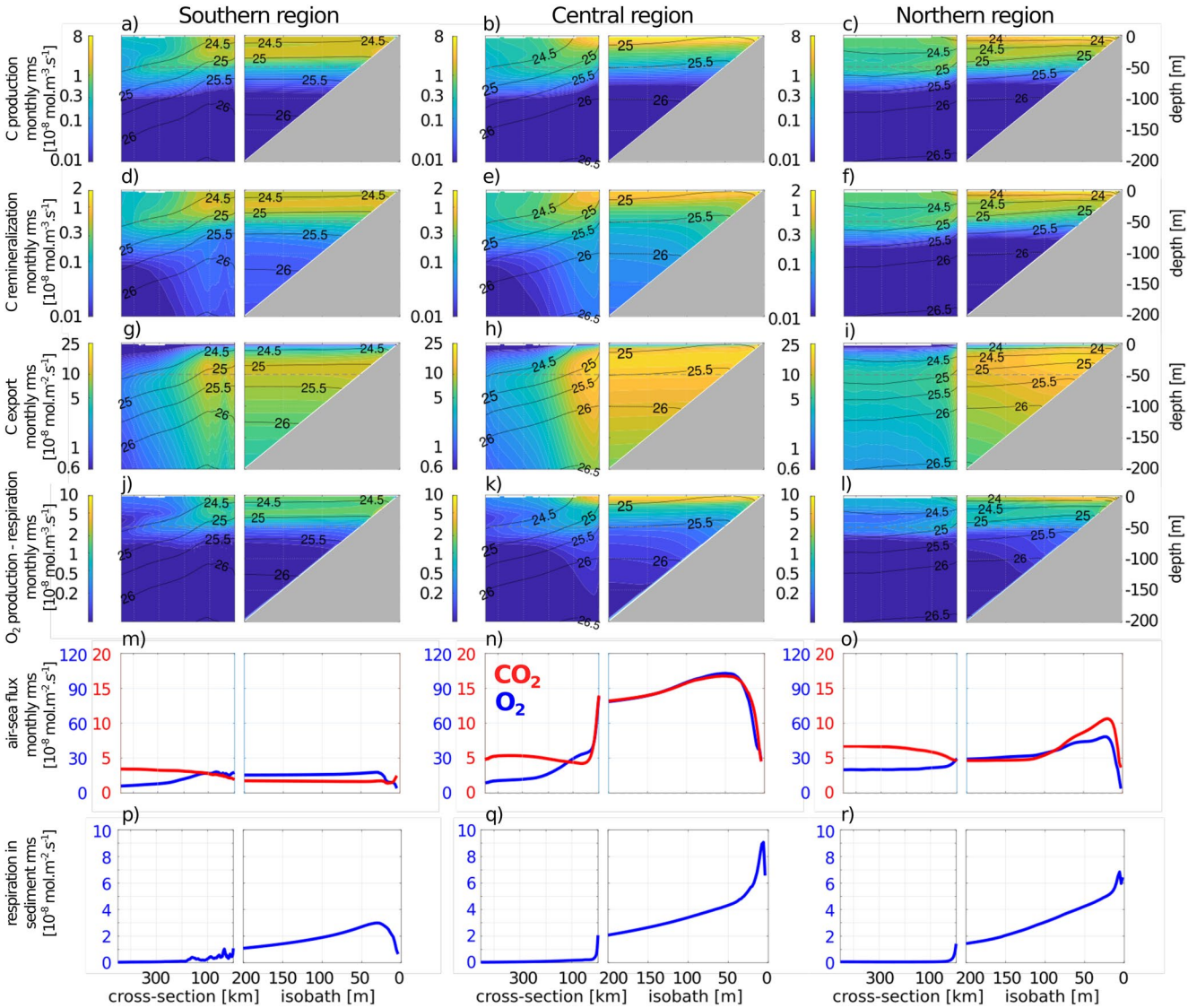

Figure B2. Vertical cross-shore sections of the monthly RMS for (a, b, c) primary production, (d, e, f) carbon remineralization, (g, h, i) particulate flux, (j, k, l) oxygen production menus respiration, (m, n, o) air-sea fluxes of (red) CO_2 and (blue) O_2, and (p, q, r) respiration in the sediment, averaged in the (left) Southern, (center) Central, and (right) Northern Regions from December 1999 to November 2007. The dashed black contours represent isopycnal surfaces with labeled potential density anomalies.

The shelf is presented as the region of intense variability of the USWC. Tracers variability increases from the Southern to the Northern Regions, reflecting the intensification of winds and seasonal cycles. It shows the largest variability in the inner shelf of the Northern Region likely driven by the seasonal reversal of the wind-driven circulation on the shelf. The same observation can be made for biogeochemical rates expect that larger variability occurs in the outter shelf of the Central Region. Off the southern continental shelf, within about 120 km of the 200 m isobath, the Southern California Bight is a secondary spot of variability. Around the islands, the subsurface variability of NO_3, DIC, and O_2 is larger than on the Southern shelf. It reflects enhanced submesoscale circulation around the Channel Islands (Dong & McWilliams, 2007).

Appendix C: Mean BGC Balances

In Figures 4 and 5, area-normalized balances are presented. Here we translate them into area-integrated balances (Figures C1 and C2). In addition, more detailed breakdowns of the mean oxygen and carbon balances are listed in Tables C1–C3.

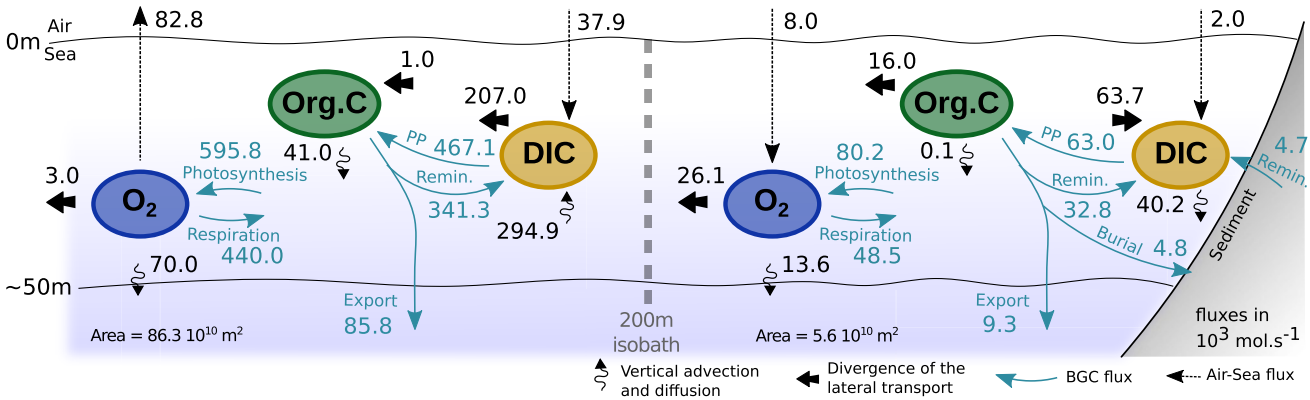

Figure C1. Spatially integrated USWC carbon and oxygen cycling schematic.

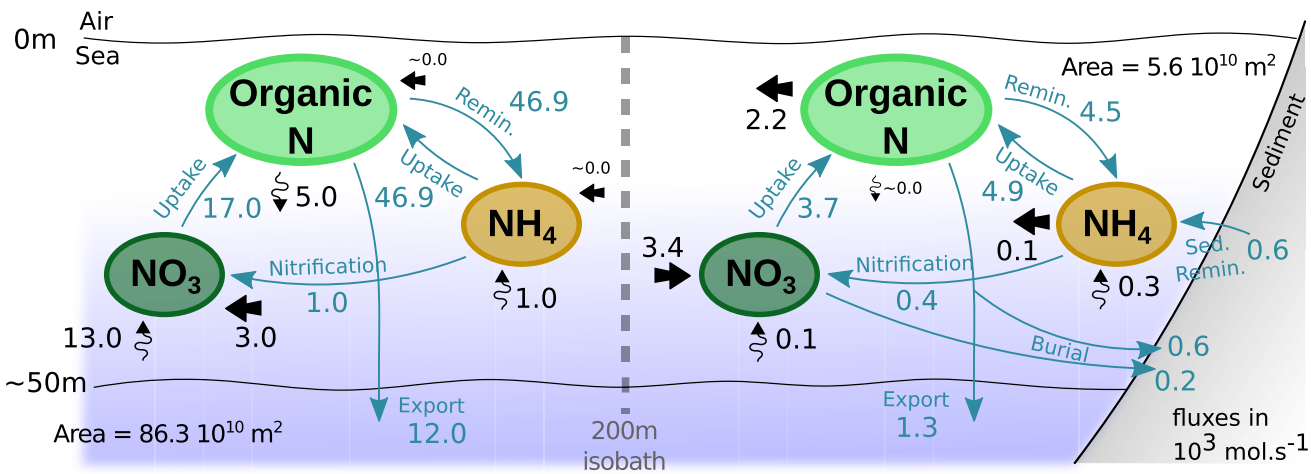

Figure C2. Spatially integrated USWC nitrogen cycling schematic.

Table C1
Details of the Mean Oxygen Balance in the USWC Upper Ocean

Oxygen balance 0–50 m (10^{-8} molO_2 m^{-2} s^{-1})										
				Southern USWC			Central USWC		Northern USWC	
	USWC	OFFSH.	SHELF	Shelf	SCB	Offshore	Shelf	Offshore	Shelf	Offshore
Area 10^{10} m^2	**91.9**	**86.3**	**5.6**	0.5	8.4	14.4	2.0	40.6	3.1	22.9
O_2 air-sea flux	**8.1**	**9.6**	**−14.5**	5.4	11.2	6.9	−48.8	12.4	4.1	5.8
Photo 0–50 m	**73.6**	**69.1**	**144.4**	129.0	98.5	44.8	183.4	78.1	122.2	57.4
Respi 0–50 m	**53.2**	**51.1**	**87.4**	83.4	67.0	37.1	97.6	56.7	81.6	43.8
VrtFlx at 50 m	**−9.1**	**−8.1**	**−24.4**	−13.6	29.4	−41.7	−15.5	−6.3	−31.9	−3.8
HrzFlx 0–50 m	**−3.2**	**−0.3**	**−47.1**	−26.6	−49.7	40.9	−119.1	−2.7	−4.6	−4.0

Note. The South California Bight (SCB) is an open embayment located in the southern region laying between the shallow shelf margin and the deep offshore ocean. It is characterized by the presence of several islands and sub-basins. Here, we define it as the region between the coastal 200 m isobath and the 2,000 m isobath on the deep slope. Bold values refer to the full USWC while unbold values refer to sub-regions.

Table C2
Details of the Mean Carbon Balance in the USWC Upper Ocean

Carbon balance 0–50 m (10^{-8} molC m^{-2} s^{-1})

				Southern USWC			Central USWC		Northern USWC	
	USWC	OFFSH.	SHELF	Shelf	SCB	Offshore	Shelf	Offshore	Shelf	Offshore
PP 0–50 m	**57.8**	**54.3**	**113.5**	101.2	77.3	35.3	144.3	61.3	96.2	45.1
CO_2 air-sea flux	**−4.4**	**−4.4**	**−3.6**	−0.8	−2.2	−0.8	5.4	−4.6	−9.8	−7.6
$Remin_C$ from sed.	**0.5**	–	**8.4**	7.8	0.2	–	12.4	–	6.1	–
Flux to sed.	**0.5**	–	**8.6**	7.9	0.2	–	12.9	–	6.1	–
$Remin_C$ 0–50 m	**40.7**	**39.6**	**59.0**	57.1	51.8	28.9	63.0	44.0	56.7	33.9
Export at 50 m	**10.4**	**10.0**	**16.8**	11.6	14.8	5.6	19.5	11.9	16.0	7.6
$HFlx_{DIC}$ 0–50 m	**−15.6**	**−24.0**	**114.9**	107.9	−413.9	296.8	53.9	−43.6	155.4	−49.3
$HFlx_{OC}$ 0–50 m	**−1.7**	**0.1**	**−28.9**	−27.5	−9.1	6.0	−49.6	0.2	−16.1	−0.6
$VrtFlx_{DIC}$ at 50 m	**27.8**	**34.2**	**−72.4**	−72.4	437.0	−291.2	20.4	56.3	−131.8	52.9
$VrtFlx_{OC}$ at 50 m	**−4.5**	**−4.7**	**−0.2**	2.9	−1.4	−6.8	0.7	−5.6	−1.3	−3.0

Table C3
Details of the Nitrogen Mean Balance in the USWC Upper Ocean

Nitrogen balance 0–50 m (10^{-8} molN m^{-2} s^{-1})

				Southern USWC			Central USWC		Northern USWC	
	USWC	OFFSH.	SHELF	Shelf	SCB	Offshore	Shelf	Offshore	Shelf	Offshore
NO_3 uptake 0–50 m	**2.2**	**2.0**	**6.6**	5.0	3.4	0.6	9.6	2.3	5.0	1.5
NH_4 uptake 0–50 m	**5.6**	**5.4**	**8.8**	8.8	7.1	4.1	10.0	6.0	8.0	4.6
Nitrif 0–50 m	**0.2**	**0.1**	**0.8**	0.3	0.2	0.0	0.9	0.2	0.8	0.2
NH_4 Remin 0–50 m	**5.6**	**5.4**	**8.0**	7.8	7.1	3.9	8.6	6.0	7.8	4.6
NH_4 Remin in sed.	**0.0**	–	**1.2**	1.0	0.0	–	1.6	–	0.8	–
Sed. denitr.	**0.0**	–	**0.4**	0.4	0.0	–	0.5	–	0.3	–
Flux to sed.	**0.0**	–	**1.2**	1.1	0.0	–	1.8	–	0.8	–
Export at 50 m	**1.4**	**1.4**	**2.3**	1.6	2.0	0.7	2.6	1.6	2.1	1.0
HFlx NO_3 0–50 m	**0.7**	**0.4**	**6.1**	6.5	−0.5	0.3	8.8	0.6	4.3	0.1
HFlx NH_4 0–50 m	**0.0**	**0.0**	**−0.1**	−0.3	0.0	0.0	−0.0	0.0	−0.2	−0.0
HFlx ON 0–50 m	**−0.2**	**0.0**	**−3.9**	−3.7	−1.2	0.8	−6.8	0.0	−2.2	−0.1
VrtFlx NO_3 at 50 m	**1.3**	**1.5**	**0.1**	−1.4	3.7	0.3	0.4	1.5	0.2	1.2
VrtFlx NH_4 at 50 m	**0.2**	**0.1**	**0.5**	0.6	0.2	0.2	0.7	0.2	0.4	0.2
VrtFlx ON at 50 m	**−0.6**	**−0.6**	**−0.0**	0.4	−0.2	−0.9	0.2	−0.7	−0.1	−0.4

Appendix D: Air-Sea Exchanges

In Figure 6, the averaged CO_2 and O_2 air-sea fluxes are presented. This mean picture is complemented by its RMS in order to evaluate their monthly variability Figure B2. In addition, we present here the monthly time series of air-sea fluxes which detailed the strong shaping by seasonal forcing (Figure D1).

In the open ocean, the air-sea flux can schematically be described as outgazing in summer and ingazing in summer. O_2 and CO_2 behave similarly likely indicating that this seasonal variability is driven by the temperature dependence of their solubility in seawater. This statement can be applied to the USWC shelf besides the seasonal intense upwelling, that is on the shelf of the Central and Northern Regions. Summer upwelling brings low-oxygen and high-DIC water toward the surface facilitating intense O_2 ingassing (up to 150×10^{-8} molO_2 m^{-2} s^{-1} on the inner shelf of the Central Region) and CO_2 outgassing (up to 20×10^{-8} molC m^{-2} s^{-1} on the inner shelf of the Central Region).

In the central region, the air-sea O_2 disequilibrium is reversed on the shelf compared to the offshore region, leading to an O_2 flux directed into the ocean on the continental margin and out of the ocean away from it. The large O_2 ingassing on the shelf can be attributed to upwelling of O_2-poor waters, which tend to rapidly equilibrate with the atmosphere via air-sea exchange. However, it appears that the upwelling-driven overturning circulation is faster than the timescale of equilibration by air-sea fluxes, so that significant surface O_2 ingassing persists on the shelf.

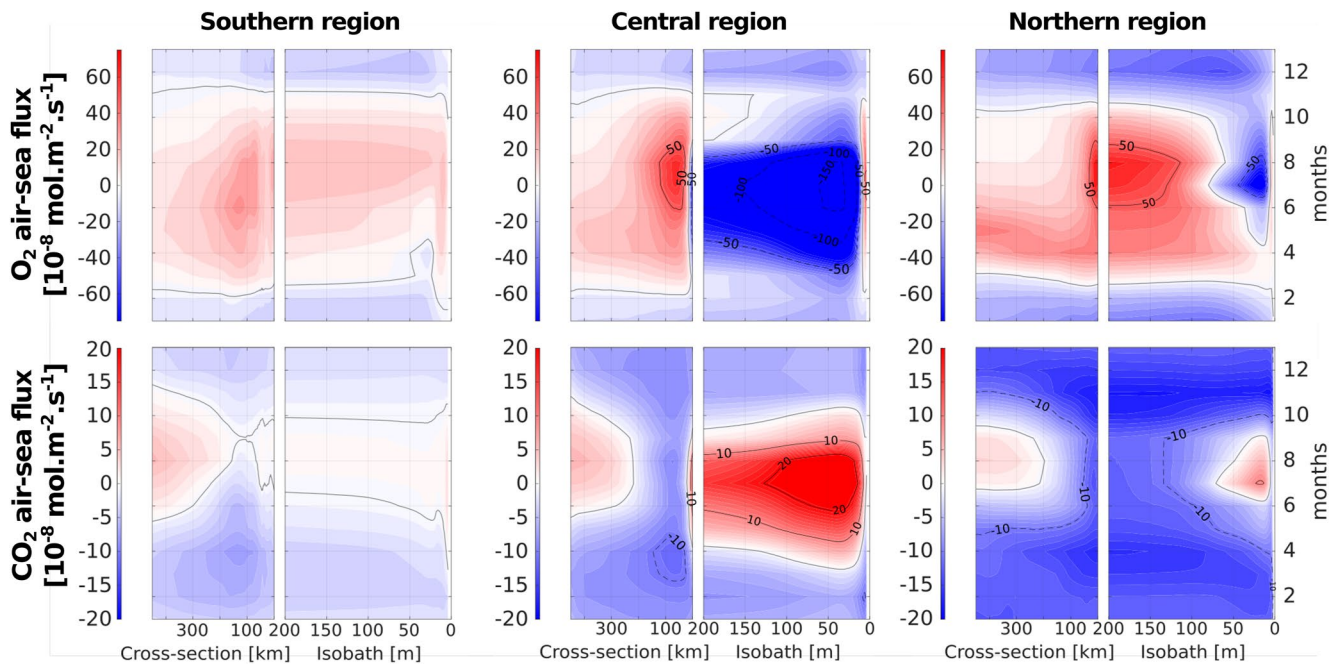

Figure D1. Seasonal variability of O_2 and CO_2 air-sea fluxes.

Appendix E: Comparison of Rate Estimates in the CCS

In order to interpret our estimates in perspective of the previous studies and validate them in the context of other findings in the literature, we present here a non-extensive summary of studies contributing to assess the biogeochemical balances along the USWC (Table E1).

The discrepancies in these independent estimates mainly arise from the varying USWC sub-regions considered by the cited references. Considering they are not point-to-point comparisons, they together provide a literature context with which our modeling results are in agreement. This gives us confidence that the model is performing reasonably well. Another important element concerns the spatial and temporal variability associated with the biogeochemical fluxes in the USWC. The reported estimates varying greatly from one sub-region to another. Also, if the variability at relatively large scales (∼for interannual to seasonal and regional) has been primarily studied in the past since it is largely forced by external mechanisms, variability at smaller scales is less known mainly due to its intrinsic and chaotic nature. In this study, we tried to reduce uncertainties by resolving biogeochemical fluxes associated with small scales processes and by producing solutions over time scales long enough to produce robust analysis.

Table E1
Comparison of BGC Rate Estimates With Selected Other Studies

Biogeochemical rate	Location		Estimates	Experiment/reference
Primary	Offshore	Central Cal.	16–67	Kahru et al. (2009)
Production		Pt. Concepcion	35–52	Stukel et al. (2011)
mmolC $m^{-2}d^{-1}$		29–34degN	19–41	Munro et al. (2013)
		USWC	46.8	*Us*
	Shelf	Pt. Concepcion	91–159	Stukel et al. (2011)
		29–34degN	53–96.7	Munro et al. (2013)
		USWC	98.1	*Us*
Carbon export	Offshore	SCB	6.4–17.0	Eppley (1992)
mmolC $m^{-2}d^{-1}$		SCB	∼27.1	Bograd et al. (2001)
		USWC	∼51.8	Messié et al. (2009)
		Pt. Concepcion	4.0–9.5	Stukel et al. (2011)
		San Pedro Basin	∼11.2	Collins et al. (2011)
		29–34degN	9.0–17.5	Munro et al. (2013)
		USWC at 200 m	4.84	*Us*
	Shelf	SCB	21.4–46.0	Eppley (1992)
		Pt. Concepcion	5.3–13.5	Stukel et al. (2011)
		29–34degN	21.4–46.6	Munro et al. (2013)
		USWC in sed.	18.9	*Us*
CO_2 air-sea flux	25–50N	370 km offshore	14	Hales et al. (2012)
$TgCyr^{-1}$	33–46N	800 km offshore	−4.5–2.7	Turi et al. (2014)
	35–50N	600 km offshore	6	Fiechter et al. (2014)
	USWC	400 km offshore	15.86	*Us*
f-ratio		Monterey Bay	0.84	Olivieri & Chavez (2000)
		Baja California	0.25–0.56	Hernández-de-la Torre et al. (2003)
		USWC shelf	0.43	*Us*
Nitrification		Monterey Bay	1–4	Ward (2005)
mmolN $m^{-2}d^{-1}$		USWC shelf	0.7	*Us*

Data Availability Statement

The model code used to generate the simulation is openly available in Kessouri, McWilliams, et al. (2020) (https://doi.org/10.5281/zenodo.3988618). Due to the size of data, model outputs can hardly be deposited on a repository but are available from the Authors upon reasonable request. The simulations are reproducible using the setup and forcing described in Section 2.1.

Acknowledgments
This research is supported by NSF grants OCE-1419323 and OCE-2023493, NOAA Grants NA15NOS4780186 and NA18NOS4780174, and California Ocean Protection Council Grants C0100400 and C0831014. Computational resources were provided by the Extreme Science and Engineering Discovery Environment (XSEDE) through allocation TG-OCE170017.

References

Banas, N. S., Lessard, E. J., Kudela, R. M., MacCready, P., Peterson, T. D., Hickey, B. M., & Frame, E. (2009). Planktonic growth and grazing in the Columbia River plume region: A biophysical model study. *Journal of Geophysical Research*, *114*(C2), C00B06. https://doi.org/10.1029/2008jc004993

Bauer, J. E., Cai, W.-J., Raymond, P. A., Bianchi, T. S., Hopkinson, C. S., & Regnier, P. A. G. (2013). The changing carbon cycle of the coastal ocean. *Nature*, *504*(7478), 61–70. https://doi.org/10.1038/nature12857

Becker, J. J., Sandwell, D. T., Smith, W. H. F., Braud, J., Binder, B., Depner, J. L., et al. (2009). Global bathymetry and elevation data at 30 arc seconds resolution: Srtm30_plus. *Marine Geodesy*, *32*(4), 355–371. https://doi.org/10.1080/01490410903297766

Bednaršek, N., Feely, R. A., Reum, J. C. P., Peterson, B., Menkel, J., Alin, S. R., & Hales, B. (2014). *Limacina helicina* shell dissolution as an indicator of declining habitat suitability owing to ocean acidification in the California Current Ecosystem. *Proceedings of the Royal Society*, *281*(1785), 20140123. https://doi.org/10.1098/rspb.2014.0123

Bograd, S. J., Chereskin, T. K., & Roemmich, D. (2001). Transport of mass, heat, salt, and nutrients in the southern California Current System: Annual cycle and interannual variability. *Journal of Geophysical Research*, *106*(C5), 9255–9275. https://doi.org/10.1029/1999jc000165

Bograd, S. J., & Mantyla, A. W. (2005). On the subduction of upwelled waters in the California current. *Journal of Marine Research*, *63*(5), 863–885. https://doi.org/10.1357/002224005774464229

Brady, R. X., Lovenduski, N. S., Yeager, S. G., Long, M. C., & Lindsay, K. (2020). Skillful multiyear predictions of ocean acidification in the California current system. *Nature Communications*, *11*, 1–9. https://doi.org/10.1038/s41467-020-15722-x

Breitburg, D., Levin, L. A., Oschlies, A., Grégoire, M., Chavez, F. P., Conley, D. J., et al. (2018). Declining oxygen in the global ocean and coastal waters. *Science*, *359*(6371). https://doi.org/10.1126/science.aam7240

Cai, W.-J. (2011). Estuarine and coastal ocean carbon paradox: CO_2 sinks or sites of terrestrial carbon incineration? *Annual Review of Marine Science*, *3*(1), 123–145. https://doi.org/10.1146/annurev-marine-120709-142723

Cai, W.-J., Hu, X., Huang, W.-J., Murrell, M. C., Lehrter, J. C., Lohrenz, S. E., et al. (2011). Acidification of subsurface coastal waters enhanced by eutrophication. *Nature Geoscience*, *4*(11), 766–770. https://doi.org/10.1038/ngeo1297

Cai, W.-J., Xu, Y.-Y., Feely, R. A., Wanninkhof, R., Jönsson, B., Alin, S. R., et al. (2020). Controls on surface water carbonate chemistry along North American ocean margins. *Nature Communications*, *11*(1), 1–13. https://doi.org/10.1038/s41467-020-16530-z

Capet, X., McWilliams, J. C., Molemaker, M. J., & Shchepetkin, A. F. (2008). Mesoscale to submesoscale transition in the California Current System. Part I: Flow structure, eddy flux, and observational tests. *Journal of Physical Oceanography*, *38*(1), 29–43. https://doi.org/10.1175/2007jpo3671.1

Chan, F., Barth, J. A., Lubchenco, J., Kirincich, A., Weeks, H., Peterson, W. T., & Menge, B. A. (2008). Emergence of anoxia in the California current large marine ecosystem. *Science*, *319*(5865), 920. https://doi.org/10.1126/science.1149016

Chavez, F. P., & Messié, M. (2009). A comparison of eastern boundary upwelling ecosystems. *Progress in Oceanography*, *83*(1–4), 80–96. https://doi.org/10.1016/j.pocean.2009.07.032

Checkley, D. M., Jr., & Barth, J. A. (2009). Patterns and processes in the California current system. *Progress in Oceanography*, *83*(1–4), 49–64. https://doi.org/10.1016/j.pocean.2009.07.028

Chenillat, F., Franks, P. J. S., Rivière, P., Capet, X., Grima, N., & Blanke, B. (2015). Plankton dynamics in a cyclonic eddy in the southern California current system. *Journal of Geophysical Research: Oceans*, *120*(8), 5566–5588. https://doi.org/10.1002/2015jc010826

Colas, F., Capet, X., McWilliams, J. C., & Li, Z. (2013). Mesoscale eddy buoyancy flux and eddy-induced circulation in eastern boundary currents. *Journal of Physical Oceanography*, *43*(6), 1073–1095. https://doi.org/10.1175/jpo-d-11-0241.1

Collins, L. E., Berelson, W., Hammond, D. E., Knapp, A., Schwartz, R., & Capone, D. (2011). Particle fluxes in San Pedro basin, California: A four-year record of sedimentation and physical forcing. *Deep-Sea Research Part I Oceanographic Research Papers*, *58*(8), 898–914. https://doi.org/10.1016/j.dsr.2011.06.008

Dai, M., Su, J., Zhao, Y., Hofmann, E. E., Cao, Z., Cai, W.-J., et al. (2022). Carbon fluxes in the coastal ocean: Synthesis, boundary processes and future trends. *Annual Review of Earth and Planetary Sciences*, *50*(1), 593–626. https://doi.org/10.1146/annurev-earth-032320-090746

Dauhajre, D. P., McWilliams, J. C., & Uchiyama, Y. (2017). Submesoscale coherent structures on the continental shelf. *Journal of Physical Oceanography*, *47*(12), 2949–2976. https://doi.org/10.1175/jpo-d-16-0270.1

Deutsch, C., Frenzel, H., McWilliams, J. C., Renault, L., Kessouri, F., Howard, E., et al. (2021). Biogeochemical variability in the California current system. *Progress in Oceanography*, *196*, 102565. https://doi.org/10.1016/j.pocean.2021.102565

Doney, S. C. (2010). The growing human footprint on coastal and open-ocean biogeochemistry. *Science*, *328*(5985), 1512–1516. https://doi.org/10.1126/science.1185198

Doney, S. C., Busch, D. S., Cooley, S. R., & Kroeker, K. J. (2020). The impacts of ocean acidification on marine ecosystems and reliant human communities. *Annual Review of Environment and Resources*, *45*(1), 83–112. https://doi.org/10.1146/annurev-environ-012320-083019

Doney, S. C., Mahowald, N., Lima, I., Feely, R. A., Mackenzie, F. T., Lamarque, J.-F., & Rasch, P. J. (2007). Impact of anthropogenic atmospheric nitrogen and sulfur deposition on ocean acidification and the inorganic carbon system. *Proceedings of the National Academy of Sciences*, *104*(37), 14580–14585. https://doi.org/10.1073/pnas.0702218104

Dong, C., & McWilliams, J. C. (2007). A numerical study of island wakes in the Southern California Bight. *Continental Shelf Research*, *27*(9), 1233–1248. https://doi.org/10.1016/j.csr.2007.01.016

Eppley, R. W. (1992). Chlorophyll, photosynthesis and new production in the Southern California Bight. *Progress in Oceanography*, *30*(1–4), 117–150. https://doi.org/10.1016/0079-6611(92)90010-w

Esaias, W. E., Abbott, M. R., Barton, I., Brown, O. B., Campbell, J. W., Carder, K. L., et al. (1998). An overview of MODIS capabilities for ocean science observations. *IEEE Transactions on Geoscience and Remote Sensing*, *36*(4), 1250–1265. https://doi.org/10.1109/36.701076

Feely, R. A., Sabine, C. L., Hernandez-Ayon, J. M., Ianson, D., & Hales, B. (2008). Evidence for upwelling of corrosive "acidified" water onto the continental shelf. *Science*, *320*(5882), 1490–1492. https://doi.org/10.1126/science.1155676

Fennel, K., Alin, S., Barbero, L., Evans, W., Bourgeois, T., Cooley, S., et al. (2019). Carbon cycling in the North American coastal ocean: A synthesis. *Biogeosciences*, *16*(6), 1281–1304. https://doi.org/10.5194/bg-16-1281-2019

Fennel, K., & Testa, J. M. (2019). Biogeochemical controls on coastal hypoxia. *Annual Review of Marine Science*, *11*(1), 105–130. https://doi.org/10.1146/annurev-marine-010318-095138

Fennel, K., Wilkin, J., Previdi, M., & Najjar, R. (2008). Denitrification effects on air-sea CO_2 flux in the coastal ocean: Simulations for the northwest North Atlantic. *Geophysical Research Letters*, *35*(24), L24608. https://doi.org/10.1029/2008gl036147

Fiechter, J., Curchitser, E. N., Edwards, C. A., Chai, F., Goebel, N. L., & Chavez, F. P. (2014). Air-sea CO_2 fluxes in the California Current: Impacts of model resolution and coastal topography. *Global Biogeochemical Cycles*, *28*(4), 371–385. https://doi.org/10.1002/2013gb004683

Fiechter, J., Edwards, C. A., & Moore, A. M. (2018). Wind, circulation, and topographic effects on alongshore phytoplankton variability in the California current. *Geophysical Research Letters*, *45*(7), 3238–3245. https://doi.org/10.1002/2017gl076839

Frenger, I., Bianchi, D., StühRenberg, C., Oschlies, A., Dunne, J., Deutsch, C., et al. (2018). Biogeochemical role of subsurface coherent eddies in the ocean: Tracer cannonballs, hypoxic storms, and microbial stewpots? *Global Biogeochemical Cycles*, *32*(2), 226–249. https://doi.org/10.1002/2017gb005743

Friederich, G. E., Walz, P. M., Burczynski, M. G., & Chavez, F. P. (2002). Inorganic carbon in the central California upwelling system during the 1997–1999 El Niño–La Niña event. *Progress in Oceanography*, *54*(1–4), 185–203. https://doi.org/10.1016/s0079-6611(02)00049-6

Frischknecht, M., Münnich, M., & Gruber, N. (2018). Origin, transformation, and fate: The three-dimensional biological pump in the California current system. *Journal of Geophysical Research: Oceans*, *123*(11), 7939–7962. https://doi.org/10.1029/2018jc013934

Garfield, N., Collins, C. A., Paquette, R. G., & Carter, E. (1999). Lagrangian exploration of the California Undercurrent, 1992–95. *Journal of Physical Oceanography*, *29*(4), 560–583. https://doi.org/10.1175/1520-0485(1999)029<0560:leotcu>2.0.co;2

Grantham, B. A., Chan, F., Nielsen, K. J., Fox, D. S., Barth, J. A., Huyer, A., et al. (2004). Upwelling-driven nearshore hypoxia signals ecosystem and oceanographic changes in the northeast Pacific. *Nature*, *429*(6993), 749–754. https://doi.org/10.1038/nature02605

Gruber, N., Hauri, C., Lachkar, Z., Loher, D., Frölicher, T. L., & Plattner, G.-K. (2012). Rapid progression of ocean acidification in the California Current System. *Science*, *337*(6091), 220–223. https://doi.org/10.1126/science.1216773

Gruber, N., Lachkar, Z., Frenzel, H., Marchesiello, P., Münnich, M., McWilliams, J. C., et al. (2011). Eddy-induced reduction of biological production in eastern boundary upwelling systems. *Nature Geoscience*, *4*(11), 787–792. https://doi.org/10.1038/ngeo1273

Hales, B., Strutton, P. G., Saraceno, M., Letelier, R., Takahashi, T., Feely, R., et al. (2012). Satellite-based prediction of pCO_2 in coastal waters of the eastern North Pacific. *Progress in Oceanography*, *103*, 1–15. https://doi.org/10.1016/j.pocean.2012.03.001

Hernández-de-la Torre, B., Gaxiola-Castro, G., Alvarez-Borrego, S., Gómez-Valdés, J., & Nájera-Martínez, S. (2003). Interannual variability of new production in the southern region of the California Current. *Deep Sea Research Part II: Topical Studies in Oceanography*, *50*(14–16), 2423–2430. https://doi.org/10.1016/s0967-0645(03)00129-2

Hickey, B. M. (1979). The California current system—Hypotheses and facts. *Progress in Oceanography*, *8*(4), 191–279. https://doi.org/10.1016/0079-6611(79)90002-8

Hickey, B. M., & Banas, N. S. (2008). Why is the northern end of the California Current System so productive? *Oceanography*, *21*(4), 90–107. https://doi.org/10.5670/oceanog.2008.07

Hofmann, E. E., Cahill, B., Fennel, K., Friedrichs, M. A. M., Hyde, K., Lee, C., et al. (2011). Modeling the dynamics of continental shelf carbon. *Annual Review of Marine Science*, *3*(1), 93–122. https://doi.org/10.1146/annurev-marine-120709-142740

Howard, E. M., Frenzel, H., Kessouri, F., Renault, L., Bianchi, D., McWilliams, J. C., & Deutsch, C. (2020). Attributing causes of future climate change in the California current system with multimodel downscaling. *Global Biogeochemical Cycles*, *34*(11), e2020GB006646. https://doi.org/10.1029/2020GB006646

Huyer, A. (1983). Coastal upwelling in the California current system. *Progress in Oceanography*, *12*(3), 259–284. https://doi.org/10.1016/0079-6611(83)90010-1

Jacox, M. G., Moore, A. M., Edwards, C. A., & Fiechter, J. (2014). Spatially resolved upwelling in the California Current System and its connections to climate variability. *Geophysical Research Letters*, *41*(9), 3189–3196. https://doi.org/10.1002/2014gl059589

Kahru, M., Kudela, R., Manzano-Sarabia, M., & Mitchell, B. G. (2009). Trends in primary production in the California Current detected with satellite data. *Journal of Geophysical Research*, *114*(C2), C02004. https://doi.org/10.1029/2008jc004979

Kämpf, J., & Chapman, P. (2016). The California current upwelling system. In *Upwelling systems of the world* (pp. 97–160). Springer.

Kessouri, F., Bianchi, D., Renault, L., McWilliams, J. C., Frenzel, H., & Deutsch, C. (2020). Submesoscale currents modulate the seasonal cycle of nutrients and productivity in the California Current System. *Global Biogeochemical Cycles*, *34*(10), e2020GB006578. https://doi.org/10.1029/2020gb006578

Kessouri, F., McWilliams, J. C., Bianchi, D., Sutula, M., Renault, L., Deutsch, C., et al. (2021). Coastal eutrophication drives acidification, oxygen loss, and ecosystem change in a major oceanic upwelling system. *Proceedings of the National Academy of Sciences of the United states of America*, *118*(21), e2018856118. https://doi.org/10.1073/pnas.2018856118

Kessouri, F., McWilliams, C. J., Deutsch, C., Renault, L., Frenzel, H., Bianchi, D., & Molemaker, J. 2020*ROMS-BEC oceanic physical and biogeochemical model code for the Southern California Current System V2020*Zenodohttps://doi.org/10.5281/zenodo.3988618

King, J. R., Agostini, V. N., Harvey, C. J., McFarlane, G. A., Foreman, M. G., Overland, J. E., et al. (2011). Climate forcing and the California current ecosystem. *ICES Journal of Marine Science*, *68*(6), 1199–1216. https://doi.org/10.1093/icesjms/fsr009

Lacroix, F., Ilyina, T., Laruelle, G. G., & Regnier, P. (2021). Reconstructing the preindustrial coastal carbon cycle through a global ocean circulation model: Was the global continental shelf already both autotrophic and a CO_2 sink? *Global Biogeochemical Cycles*, *35*(2), e2020GB006603. https://doi.org/10.1029/2020gb006603

Lacroix, F., Ilyina, T., Mathis, M., Laruelle, G. G., & Regnier, P. (2021). Historical increases in land-derived nutrient inputs may alleviate effects of a changing physical climate on the oceanic carbon cycle. *Global Change Biology*, *27*(21), 5491–5513. https://doi.org/10.1111/gcb.15822

Landschützer, P., Laruelle, G. G., Roobaert, A., & Regnier, P. (2020). A uniform pCO_2 climatology combining open and coastal oceans. *Earth System Science Data*, *12*(4), 2537–2553. https://doi.org/10.5194/essd-12-2537-2020

Large, W. B. (2006). Surface fluxes for practitioners of global ocean data assimilation. *Ocean Weather Forecasting*, 229–270. https://doi.org/10.1007/1-4020-4028-8_9

Large, W. G., McWilliams, J. C., & Doney, S. C. (1994). Oceanic vertical mixing: A review and a model with a nonlocal boundary layer parameterization. *Reviews of Geophysics*, *32*(4), 363–403. https://doi.org/10.1029/94rg01872

Laruelle, G. G., Cai, W.-J., Hu, X., Gruber, N., Mackenzie, F. T., & Regnier, P. (2018). Continental shelves as a variable but increasing global sink for atmospheric carbon dioxide. *Nature Communications*, *9*(1), 1–11. https://doi.org/10.1038/s41467-017-02738-z

Laruelle, G. G., Dürr, H. H., Lauerwald, R., Hartmann, J., Slomp, C., Goossens, N., & Regnier, P. (2013). Global multi-scale segmentation of continental and coastal waters from the watersheds to the continental margins. *Hydrology and Earth System Sciences*, *17*(5), 2029–2051. https://doi.org/10.5194/hess-17-2029-2013

Laruelle, G. G., Lauerwald, R., Pfeil, B., & Regnier, P. (2014). Regionalized global budget of the CO_2 exchange at the air-water interface in continental shelf seas. *Global Biogeochemical Cycles*, *28*(11), 1199–1214. https://doi.org/10.1002/2014gb004832

Lathuilière, C., Echevin, V., Lévy, M., & Madec, G. (2010). On the role of the mesoscale circulation on an idealized coastal upwelling ecosystem. *Journal of Geophysical Research*, *115*(C9), C09016. https://doi.org/10.1029/2009jc005827

Lemarié, F., Debreu, L., Shchepetkin, A. F., & Mcwilliams, J. C. (2012). On the stability and accuracy of the harmonic and biharmonic isoneutral mixing operators in ocean models. *Ocean Modelling*, *52*, 9–35. https://doi.org/10.1016/j.ocemod.2012.04.007

Lentz, S. J., & Chapman, D. C. (2004). The importance of nonlinear cross-shelf momentum flux during wind-driven coastal upwelling. *Journal of Physical Oceanography*, *34*(11), 2444–2457. https://doi.org/10.1175/jpo2644.1

Lévy, M., Franks, P. J. S., & Smith, K. S. (2018). The role of submesoscale currents in structuring marine ecosystems. *Nature Communications*, *9*, 1–16. https://doi.org/10.1038/s41467-018-07059-3

Liu, X., Dunne, J. P., Stock, C. A., Harrison, M. J., Adcroft, A., & Resplandy, L. (2019). Simulating water residence time in the coastal ocean: A global perspective. *Geophysical Research Letters*, *46*(23), 13910–13919. https://doi.org/10.1029/2019gl085097

Liu, X., Stock, C. A., Dunne, J. P., Lee, M., Shevliakova, E., Malyshev, S., & Milly, P. C. (2021). Simulated global coastal ecosystem responses to a half-century increase in river nitrogen loads. *Geophysical Research Letters*, *48*(17), e2021GL094367. https://doi.org/10.1029/2021gl094367

Liu, Atkinson, L., Quiñones, R. A., & Talaue-McManus, L. (2010). Biogeochemistry of continental margins in a global context. In *Carbon and nutrient fluxes in continental margins* (pp. 3–24). Springer.

Lovecchio, E., Gruber, N., & Münnich, M. (2018). Mesoscale contribution to the long-range offshore transport of organic carbon from the Canary Upwelling System to the open North Atlantic. *Biogeosciences*, *15*(16), 5061–5091. https://doi.org/10.5194/bg-15-5061-2018

Lovecchio, E., Gruber, N., Münnich, M., & Lachkar, Z. (2017). On the long-range offshore transport of organic carbon from the canary upwelling system to the open north Atlantic. *Biogeosciences*, *14*(13), 3337–3369. https://doi.org/10.5194/bg-14-3337-2017

Marchesiello, P., Debreu, L., & Couvelard, X. (2009). Spurious diapycnal mixing in terrain-following coordinate models: The problem and a solution. *Ocean Modelling*, *26*, 156–169.

Marchesiello, P., McWilliams, J. C., & Shchepetkin, A. (2003). Equilibrium structure and dynamics of the California current system. *Journal of Physical Oceanography*, *33*(4), 753–783. https://doi.org/10.1175/1520-0485(2003)33<753:esadot>2.0.co;2

Marshall, K. N., Kaplan, I. C., Hodgson, E. E., Hermann, A., Busch, D. S., McElhany, P., et al. (2017). Risks of ocean acidification in the California Current food web and fisheries: Ecosystem model projections. *Global Change Biology*, *23*(4), 1525–1539. https://doi.org/10.1111/gcb.13594

McClatchie, S. (2014). *Fisheries stock assessment, environmental variability, and CalCOFI* (pp. 151–164). Regional Fisheries Oceanography of the California Current System.

McCoy, D., Bianchi, D., & Stewart, A. L. (2020). Global observations of submesoscale coherent vortices in the ocean. *Progress in Oceanography*, *189*, 102452. https://doi.org/10.1016/j.pocean.2020.102452

McWilliams, J. C. (2016). Submesoscale currents in the ocean. *Proceedings of the Royal Society A: Mathematical, Physical & Engineering Sciences*, *472*(2189), 20160117. https://doi.org/10.1098/rspa.2016.0117

Messié, M., Ledesma, J., Kolber, D. D., Michisaki, R. P., Foley, D. G., & Chavez, F. P. (2009). Potential new production estimates in four eastern boundary upwelling ecosystems. *Progress in Oceanography*, *83*(1–4), 151–158. https://doi.org/10.1016/j.pocean.2009.07.018

Molemaker, M. J., McWilliams, J. C., & Dewar, W. K. (2015). Submesoscale instability and generation of mesoscale anticyclones near a separation of the California Undercurrent. *Journal of Physical Oceanography*, *45*(3), 613–629. https://doi.org/10.1175/jpo-d-13-0225.1

Moore, J. K., Doney, S. C., & Lindsay, K. (2004). Upper ocean ecosystem dynamics and iron cycling in a global three-dimensional model. *Global Biogeochemical Cycles*, *18*(4), 18. https://doi.org/10.1029/2004gb002220

Muller-Karger, F. E., Varela, R., Thunell, R., Luerssen, R., Hu, C., & Walsh, J. J. (2005). The importance of continental margins in the global carbon cycle. *Geophysical Research Letters*, *32*(1), L01602. https://doi.org/10.1029/2004gl021346

Munro, D. R., Quay, P. D., Juranek, L. W., & Goericke, R. (2013). Biological production rates off the southern California coast estimated from triple O_2 isotopes and O_2: Ar gas ratios. *Limnology & Oceanography*, *58*(4), 1312–1328. https://doi.org/10.4319/lo.2013.58.4.1312

Nagai, T., Gruber, N., Frenzel, H., Lachkar, Z., McWilliams, J. C., & Plattner, G.-K. (2015). Dominant role of eddies and filaments in the offshore transport of carbon and nutrients in the California Current System. *Journal of Geophysical Research: Oceans*, *120*(8), 5318–5341. https://doi.org/10.1002/2015jc010889

Najjar, R. G., Herrmann, M., Alexander, R., Boyer, E. W., Burdige, D., Butman, D., et al. (2018). Carbon budget of tidal wetlands, estuaries, and shelf waters of eastern North America. *Global Biogeochemical Cycles*, *32*(3), 389–416. https://doi.org/10.1002/2017gb005790

Olivieri, R. A., & Chavez, F. P. (2000). A model of plankton dynamics for the coastal upwelling system of Monterey Bay, California. *Deep Sea Research Part II: Topical Studies in Oceanography*, *47*(5–6), 1077–1106. https://doi.org/10.1016/s0967-0645(99)00137-x

Osborne, E. B., Thunell, R. C., Gruber, N., Feely, R. A., & Benitez-Nelson, C. R. (2020). Decadal variability in twentieth-century ocean acidification in the California current ecosystem. *Nature Geoscience*, *13*(1), 43–49. https://doi.org/10.1038/s41561-019-0499-z

Perlin, A., Moum, J. N., & Klymak, J. M. (2005). Response of the bottom boundary layer over a sloping shelf to variations in alongshore wind. *Journal of Geophysical Research*, *110*(C10), C10S09. https://doi.org/10.1029/2004jc002500

Pespeni, M. H., Chan, F., Menge, B. A., & Palumbi, S. R. (2013). Signs of adaptation to local PH conditions across an environmental mosaic in the California Current Ecosystem. *Integrative and Comparative Biology*, *53*(5), 857–870. https://doi.org/10.1093/icb/ict094

Pozo Buil, M., Jacox, M. G., Fiechter, J., Alexander, M. A., Bograd, S. J., Curchitser, E. N., et al. (2021). A dynamically downscaled ensemble of future projections for the California current system. *Frontiers in Marine Science*, *8*, 612874. https://doi.org/10.3389/fmars.2021.612874

Regnier, P., Friedlingstein, P., Ciais, P., Mackenzie, F. T., Gruber, N., Janssens, I. A., et al. (2013). Anthropogenic perturbation of the carbon fluxes from land to ocean. *Nature Geoscience*, *6*(8), 597–607. https://doi.org/10.1038/ngeo1830

Regnier, P., Resplandy, L., Najjar, R. G., & Ciais, P. (2022). The land-to-ocean loops of the global carbon cycle. *Nature*, *603*(7901), 401–410. https://doi.org/10.1038/s41586-021-04339-9

Renault, L., Deutsch, C., McWilliams, J. C., Frenzel, H., Liang, J.-H., & Colas, F. (2016). Partial decoupling of primary productivity from upwelling in the California current system. *Nature Geoscience*, *9*(7), 505–508. https://doi.org/10.1038/ngeo2722

Renault, L., Hall, A., & McWilliams, J. C. (2016). Orographic shaping of us west coast wind profiles during the upwelling season. *Climate Dynamics*, *46*(1–2), 273–289. https://doi.org/10.1007/s00382-015-2583-4

Renault, L., Masson, S., Arsouze, T., Madec, G., & McWilliams, J. C. (2020). Recipes for how to force oceanic model dynamics. *Journal of Advances in Modeling Earth Systems*, *12*(2), e2019MS001715. https://doi.org/10.1029/2019ms001715

Renault, L., McWilliams, J. C., Jousse, A., Deutsch, C., Frenzel, H., Kessouri, F., & Chen, R. (2021). The physical structure and behavior of the California current system. *Progress in Oceanography*, *195*, 102564. https://doi.org/10.1016/j.pocean.2021.102564

Renault, L., Molemaker, M. J., McWilliams, J. C., Shchepetkin, A. F., Lemarié, F., Chelton, D., et al. (2016). Modulation of wind work by oceanic current interaction with the atmosphere. *Journal of Physical Oceanography*, *46*(6), 1685–1704. https://doi.org/10.1175/jpo-d-15-0232.1

Roobaert, A., Laruelle, G. G., Landschützer, P., Gruber, N., Chou, L., & Regnier, P. (2019). The spatiotemporal dynamics of the sources and sinks of CO_2 in the global coastal ocean. *Global Biogeochemical Cycles*, *33*(12), 1693–1714. https://doi.org/10.1029/2019gb006239

Shchepetkin, A. F., & McWilliams, J. C. (2005). The regional oceanic modeling system (ROMS): A split-explicit, free-surface, topography-following-coordinate oceanic model. *Ocean Modelling*, *9*(4), 347–404. https://doi.org/10.1016/j.ocemod.2004.08.002

Shchepetkin, A. F., & McWilliams, J. C. (2009). Correction and commentary for "Ocean forecasting in terrain-following coordinates: Formulation and skill assessment of the regional ocean modeling system" by Haidvogel et al., J. Comp. Phys. 227, pp. 3595–3624. *Journal of Computational Physics*, *228*(24), 8985–9000. https://doi.org/10.1016/j.jcp.2009.09.002

Skamarock, W. C., Klemp, J. B., Dudhia, J., Gill, D. O., Barker, D. M., Duda, M. G., et al. (2008). G.: A description of the advanced research WRF version 3. NCAR Tech. Note NCAR/TN-475+ STR.

Stock, C. A., Dunne, J. P., Fan, S., Ginoux, P., John, J., Krasting, J. P., et al. (2020). Ocean biogeochemistry in GFDL's Earth system model 4.1 and its response to increasing atmospheric CO_2. *Journal of Advances in Modeling Earth Systems*, *12*(10), e2019MS002043. https://doi.org/10.1029/2019ms002043

Stukel, M. R., Landry, M. R., Benitez-Nelson, C. R., & Goericke, R. (2011). Trophic cycling and carbon export relationships in the California current ecosystem. *Limnology & Oceanography*, *56*(5), 1866–1878. https://doi.org/10.4319/lo.2011.56.5.1866

Sutula, M., Ho, M., Sengupta, A., Kessouri, F., McLaughlin, K., McCune, K., & Bianchi, D. (2021). A baseline of terrestrial freshwater and nitrogen fluxes to the southern California bight, USA. *Marine Pollution Bulletin*, *170*, 112669. https://doi.org/10.1016/j.marpolbul.2021.112669

Thomas, L. N., Tandon, A., & Mahadevan, A. (2008). Submesoscale processes and dynamics. Ocean modeling in an eddying regime. *Geophysical Monograph Series*, *177*, 17–38.

Turi, G., Lachkar, Z., & Gruber, N. (2014). Spatiotemporal variability and drivers of pCO_2 and air–sea CO_2 fluxes in the California current system: An eddy-resolving modeling study. *Biogeosciences*, *11*(3), 671–690. https://doi.org/10.5194/bg-11-671-2014

Villacieros-Robineau, N., Zúñiga, D., Barreiro-González, B., Alonso-Pérez, F., de la Granda, F., Froján, M., et al. (2019). Bottom boundary layer and particle dynamics in an upwelling affected continental margin (NW Iberia). *Journal of Geophysical Research: Oceans*, *124*(12), 9531–9552. https://doi.org/10.1029/2019jc015619

Walsh, J. J. (1991). Importance of continental margins in the marine biogeochemical cycling of carbon and nitrogen. *Nature*, *350*(6313), 53–55. https://doi.org/10.1038/350053a0

Ward, B. B. (2005). Temporal variability in nitrification rates and related biogeochemical factors in Monterey Bay, California, USA. *Marine Ecology Progress Series*, *292*, 97–109. https://doi.org/10.3354/meps292097